

Cosmological constraints from the DESI DR1 joint power spectrum and bispectrum analysis

S. Novell-Masot,^{1,2} H. Gil-Marín^{3,4,1} , L. Verde^{5,1} , J. Aguilar,⁶
S. Ahlen⁷ , D. Bianchi^{8,9} , D. Brooks,¹⁰ F. J. Castander^{4,11} ,
T. Claybaugh,⁶ S. Cole¹² , A. de la Macorra¹³ ,
J. Della Costa¹⁴ , S. Ferraro^{6,15} , A. Font-Ribera^{5,16} ,
J. E. Forero-Romero^{17,18} , E. Gaztañaga^{4,19,11} , S. Gontcho A
Gontcho²⁰ , A. X. Gonzalez-Morales²¹ , G. Gutierrez,²²
J. Guy⁶ , C. Hahn²³ , H. K. Herrera-Alcantar^{24,25} ,
K. Honscheid^{26,27,28} , C. Howlett²⁹ , M. Ishak³⁰ ,
J. Jimenez¹⁶ , R. Joyce¹⁴ , R. Kehoe,³¹ D. Kirkby³² ,
A. Kremin⁶ , C. Lamman²⁸ , L. Le Guillou³³ , M. Manera^{34,16} ,
A. Meisner¹⁴ , R. Miquel,^{5,16} S. Nadathur¹⁹ , G. Niz^{21,35} ,
W. J. Percival^{36,37,38} , I. Pérez-Ràfols³⁹ , G. Rossi,⁴⁰
L. Samushia^{41,42,43} , E. Sanchez⁴⁴ , E. F. Schlafly⁴⁵ ,
D. Schlegel,⁶ M. Schubnell,^{46,47} J. Silber⁶ , D. Sprayberry,¹⁴
G. Tarlé⁴⁷ , B. A. Weaver,¹⁴ C. Zhao⁴⁸ , R. Zhou⁶ 

Affiliations are in Appendix C

E-mail: sergi.novell@icc.ub.edu, hectorgil@icc.ub.edu, liciaverde@icc.ub.edu

Abstract. We derive cosmological parameter constraints from the Dark Energy Spectroscopic Instrument (DESI) Data Release 1 (DR1) galaxy clustering data, based on a joint full-shape analysis of the power spectrum multipoles and the bispectrum monopole using the ShapeFit framework [1]. This work is the follow-up of [2], which obtains for the first time constraints on the ShapeFit parameters using the bispectrum of DESI DR1, for the luminous red galaxy (LRG) and quasar (QSO) samples. Here we present the first ShapeFit cosmological inference results using the bispectrum of DESI DR1. For the baseline flat Λ CDM model, our analysis yields results broadly in agreement with previous studies of the DESI DR1 data-set. In particular, we recover values for the matter density parameter and Hubble constant of respectively $\Omega_m = 0.310 \pm 0.012$ and $H_0 = [68.92 \pm 0.97] \text{ km s}^{-1} \text{ Mpc}^{-1}$, consistent with previous results from the full DESI DR1 dataset that did not use the bispectrum signal [3]. The inclusion of the bispectrum significantly tightens the constraints on the amplitude of fluctuations, reducing the error-bars in $\ln(A_s \times 10^{10})$ by approximately 20%, compared to using the power spectrum alone. We also explore extended cosmological models by performing fits for the evolving dark energy equation of state $w_0 w_a$, and the sum of neutrino masses $\sum m_\nu$. In these cases, we obtain constraints slightly larger than the ones from previous works from the DESI collaboration [4], due to not combining the full-shape results with other probes in all tracers. We find no strong evidence of deviations from standard Λ CDM, with the dark energy equation-of-state remaining within 2σ from a cosmological constant Λ , and the neutrino mass being consistent with the normal hierarchy, $\sum m_\nu < 0.1 \text{ [eV]}$ at 95% confidence limit. These constraints are broadly consistent with other DESI DR1 analyses, thus validating the robustness of the ShapeFit compression approach and the inclusion of the bispectrum for cosmological inference.

Contents

1	Introduction	1
2	Methodology	3
2.1	ShapeFit compression.	3
2.2	Data and measurements.	4
2.3	Cosmological parameter inference.	5
3	Results	6
3.1	Baseline Λ CDM results	6
3.2	Sound-horizon marginalization	8
3.3	Evolving dark energy (w_0w_a)	9
3.4	Neutrino mass constraints	11
4	Discussion	12
A	The ShapeFit Interpretation Vademecum	15
B	Sequential ShapeFit compression	17
C	Author Affiliations	19

1 Introduction

Increasingly large and high-precision cosmological datasets are allowing for even more stringent tests of the cosmological model. The Λ -Cold Dark Matter (Λ CDM) framework has been remarkably successful at explaining observations across cosmic history [5]. Yet, challenges remain, including the unknown nature of the dark components (dark matter and dark energy) that dominate the energy density of the Universe, as well as observed tensions between early- and late-Universe measurements [4, 6, 7]. These persistent issues motivate the continued exploration of potential new physics beyond Λ CDM.

Galaxy redshift surveys have become one of the primary ways of probing the large-scale structure (LSS) of the Universe. Surveys such as the Sloan Digital Sky Survey (SDSS) [8], the 2-degree Field Galaxy Redshift Survey (2dfGRS) [9], the Baryon Oscillation Spectroscopic Survey (BOSS) [10], and the extended BOSS (eBOSS) [11] successfully obtained LSS cosmological constraints from increasingly larger datasets.

Building on this, the Dark Energy Spectroscopic Instrument (DESI) [7, 12–28] is obtaining spectra for more than 60 million objects [29], including luminous red galaxies (LRG) [20], emission-line galaxies (ELG) [30], and quasars (QSO) [31], as well as the nearby bright galaxy survey (BGS) [32] and the high redshift Lyman- α forest [24]. DESI is mapping a cosmological volume many times larger than all previous surveys combined, which enables exquisite precision in the measurement of the traditional signatures in LSS cosmology, namely, baryon acoustic oscillation (BAO) and redshift-space distortions (RSD). The density of tracers measured by DESI provides enough statistical power to perform analyses beyond two-point, which is key to break parameter degeneracies, tighten cosmological constraints and provide additional tests for Λ CDM [33–53]. Indeed, even though higher-order statistics such as the

bispectrum or three-point correlation function have been long studied, only a few works applied them to galaxy surveys [49, 54–65].

The information contained in the BAO and RSD signals of the galaxy catalogue summary statistics (such as the power spectrum or the bispectrum) constitutes only *a partial* set of the whole information contained in those statistics. Standard BAO and RSD analyses marginalize over features present in the broadband shape of $P(k)$, focusing on two robust observables: the BAO scale –often parametrized by the dilation factors $\alpha_{\parallel}, \alpha_{\perp}$ along and across the line of sight, respectively– and the product of the logarithmic growth rate f and the averaged amplitude of perturbations σ_8 . While this *compressed* approach has the virtue of being largely model-independent, it is not able to capture the full information enclosed in the power spectrum. One way to do so is through the so-called Full Modelling analysis of the power spectrum (sometimes called “direct fit”), which fits the power spectrum directly from the theoretical predictions for any given cosmology. Such an approach yields tighter constraints by exploiting information enclosed in the broadband shape of the matter power spectrum. However, the most popular implementation of such analysis requires adopting informative priors over poorly known nuisance parameters.

The ShapeFit methodology [1, 66–68] was proposed as a middle ground between the standard BAO-RSD compression and a Full Modelling analysis. In a ShapeFit-based analysis, one still performs a template fit to the galaxy power spectrum, but includes two additional parameters (m, n) that model the slope of the power spectrum near the matter-radiation equality scale. After obtaining constraints for the full set of ShapeFit parameters and performing cosmological inference on them, one can recover results with statistical power close to those of direct full-shape fits for models close to Λ CDM [66] and its popular extensions [69–73].

In our previous work [2], we applied the ShapeFit compression technique to the clustering data from DESI DR1. In particular, we constrained the ShapeFit parameters using the power spectrum and bispectrum statistics in the LRG and QSO tracers, spanning redshifts between $0.4 < z < 2.5$. We obtained joint power spectrum-bispectrum results highly compatible with the power spectrum-only analysis from the DESI collaboration [3], with the addition of the bispectrum yielding tighter constraints, as well as disentangling the f and σ_8 parameters.

In this work, we use the results from that analysis to infer cosmological constraints under various model assumptions. Because the ShapeFit compression is model-agnostic, constraints on the compressed variables can simply be re-interpreted within the chosen cosmological model. In particular, we start by obtaining the Λ CDM results from the ShapeFit constraints with and without the inclusion of the bispectrum. We also compare our main approach (using power spectrum and bispectrum) with the analogous case using the traditional BAO+RSD results, to highlight the effect of adding the shape parameter in the analysis.

Then, we obtain sound horizon-free constraints for the Ω_m and H_0 parameters, in which we interpret the BAO signal without assuming the sound-horizon scale r_d from early-time physics. We also explore other relevant cosmological models, constraining the time-varying dark energy equation of state (using the Chevallier-Polarski-Linder (CPL) parametrization with w_0 and w_a [74, 75]), and the total neutrino mass $\sum m_\nu$.

This paper is organized as follows. In Section 2 we describe the data and the ShapeFit methodology and measurements, including details of the ShapeFit implementation and the cosmological parameter inference procedure. Section 3 presents our results: we first discuss the baseline Λ CDM constraints (Section 3.1). We then report the findings for each extended scenario: sound-horizon marginalization (Section 3.2), evolving dark energy (Section 3.3),

and neutrino mass (Section 3.4). In Section 4, we discuss the implications of our results and conclude.

2 Methodology

2.1 ShapeFit compression.

Following the ShapeFit methodology described in [1, 68], rather than directly performing a direct fit of a cosmological model to the measured power spectra and bispectra, we first compress the data into a set of intermediate compressed parameters. The full details of this procedure and parameters can be found in [2]. In short, for each galaxy sample and redshift bin, we fit the joint power spectrum-bispectrum data-vector to a template based on a reference (or fiducial) cosmology, obtaining constraints for the following parameters (see appendix A for a concise summary on the ShapeFit variables and their connection to the cosmological variables):

- $\alpha_{\text{iso}}(z)$: the isotropic BAO scaling, defined as the ratio of $D_V(z)/r_d$ relative to the fiducial or reference cosmology, $\alpha_{\text{iso}}(z) = [D_V(z)/r_d]/[D_V(z)/r_d]^{\text{ref}}$. The volume distance $D_V(z)$ is appropriately defined as $D_V(z) = (zD_M(z)^2D_H(z))^{1/3}$, with $D_M(z)$ the angular diameter distance and $D_H(z) \equiv c/H(z)$ the Hubble distance. Hence, $\alpha_{\text{iso}}(z)$ encodes information from both late-time (via $D_V(z)$) and early-time (via r_d) physics.
- $\alpha_{\text{AP}}(z)$: the anisotropic Alcock-Paczynski distortion parameter, sensitive to the ratio of the Hubble distance and the angular diameter distance: $\alpha_{\text{AP}}(z) = [D_H(z)/D_M(z)]/[D_H(z)/D_M(z)]^{\text{ref}}$, which is therefore a purely late-time quantity.
- $\sigma_{\text{ss}}(z)$: The amplitude of matter fluctuations at redshift z , smoothed on the scale of $8r_d^{\text{ref}}r_d^{-1}\text{Mpch}^{-1}$. Note the change from the usual name σ_8 to σ_{ss} : In the case of σ_8 , the smoothing is on the constant scale 8Mpch^{-1} (making it dependent on dilations of scale, which are parametrized by $\alpha_{\text{iso}}(z)$, $\alpha_{\text{AP}}(z)$)—more details in Section 3 of [1].
- $f(z)$: The logarithmic growth rate of structure. This quantity, in a ΛCDM cosmology under the assumption of general relativity, is uniquely determined by Ω_m , as $f(z) = \Omega_m(z)^{0.55}$. In non- ΛCDM , but still GR, models $f(z)$ is uniquely determined by $\Omega_m(z)$ and background quantities, while on non-GR models, this is not the case.

In two-point analyses, $f(z)$ is highly degenerate with $\sigma_{\text{ss}}(z)$, as the amplitude of two-point clustering is proportional to the product $f\sigma_{\text{ss}}(z)$. The addition of the bispectrum statistic allows constraining $f(z)$ separately by breaking the degeneracy.

- $m(z) + n(z)$: the combined ShapeFit parameter, obtained as the sum of two different parameters affecting the slope of the power spectrum. The parameter $m(z)$ governs the slope of the power spectrum around the matter-radiation equality scale, while $n(z)$ models variations of the primordial spectral index. These two parameters are highly degenerate for current data sets, and using their sum (which is equivalent to m -at-fixed- n , or vice versa) compresses the information of both parameters without perceptible loss, as reported in figure 9 of [76].

When only $\{\alpha_{\text{iso}}, \alpha_{\text{AP}}, f, \sigma_{\text{ss}}\}$ are employed, we refer to the analysis as a BAO+RSD (or Standard Compression), whereas when $m + n$ is also added, we refer to it as a ShapeFit analysis. In appendix B we display how the cosmological inference for ΛCDM for the dataset

described in Table 1 compares when using the full set of variables above (ShapeFit), or when using a subset of it: *i*) shape variables $m + n$ only; and *ii*) α_{iso} , α_{AP} and $f\sigma_{\text{s8}}$ mimicking the traditional compression analysis).

The pipeline used to constrain the compressed parameters is calibrated exclusively on blinded data [77–79]. It accounts for the effects of the survey window [80] and incorporates the full systematic error budget into the reported uncertainties.

The power spectrum model is based on two-loop renormalized perturbation theory (RPT) [56, 81], the bispectrum is modelled with GEO-FPT [82], and the covariance matrices are estimated from large sets of mock catalogs [83, 84]. Therefore, we fully account for "real-world" effects, including the cross-correlation terms between the power spectrum and the bispectrum. More details can be found in [2, 84].

2.2 Data and measurements.

The DESI DR1 is divided into several redshift bins, according to the corresponding tracer: the bright galaxy survey, BGS [32]; the luminous red galaxies [20], LRG, which are split in the three redshift bins LRG1, LRG2, LRG3; emission line galaxies [30], ELG, divided in two redshift bins ELG1 and ELG2; and quasars (QSO) [31], as well as the Lyman- α forest data [24]. Summary information about these tracers can be found in Table 1.

Tracer	Redshift range	N_{tracer}	z_{eff}	$P_0 [(\text{Mpc}h^{-1})^3]$	$V_{\text{eff}} [\text{Gpc}^3]$	Used in this work as
BGS	0.1 – 0.4	300,017	0.295	$\sim 9.2 \times 10^3$	1.7	BAO recon.
LRG1	0.4 – 0.6	506,905	0.510	$\sim 8.9 \times 10^3$	2.6	FS
LRG2	0.6 – 0.8	771,875	0.706	$\sim 8.9 \times 10^3$	4.0	FS
LRG3	0.8 – 1.1	859,824	0.920	$\sim 8.4 \times 10^3$	5.0	FS
ELG1	0.8 – 1.1	1,016,340	0.955	$\sim 2.6 \times 10^3$	2.0	BAO recon.
ELG2	1.1 – 1.6	1,415,687	1.317	$\sim 2.9 \times 10^3$	2.7	BAO recon.
QSO	0.8 – 2.1	856,652	1.491	$\sim 5.0 \times 10^3$	1.5	FS

Table 1. Main properties of the DESI DR1 tracers: redshift range, counts per redshift bin, effective redshift z_{eff} , power spectrum monopole amplitude at the reference scale of $k = 0.14 h\text{Mpc}^{-1}$, P_0 , and effective volume V_{eff} . We use the full-shape results from the joint power spectrum and bispectrum analysis of [2] for the three LRG bins and the QSOs, while using reconstructed BAO constraints for the BGS and the ELG samples from [23]. Additionally, we also use the Lyman- α BAO measurements from [24].

In this work, we utilise the ShapeFit constraints for the three LRG bins and the QSOs obtained by using the joint power spectrum and bispectrum analysis performed in [2]. These constraints were obtained by using the power spectrum multipoles and bispectrum monopole, where in the LRG bins the power spectrum multipoles include monopole, quadrupole and hexadecapole. For the QSO tracers, we did not use the power spectrum hexadecapole due to the lower signal present in that case (see figure 13 of [2] to show how the inclusion of the hexadecapole does not significantly improve the constraining power for the QSO sample). Ref [2] does not perform a bispectrum analysis on the ELG sample because of large imaging systematics and the difficulty in correcting them at the level of the bispectrum signal; the BGS bispectrum analysis was not performed due to its lower effective volume and limited constraining power. Additionally, the DR1 BAO reconstruction signal is only employed in those bins where we do not have a ShapeFit power spectrum and bispectrum measurement (ELG and BGS). Although we could have employed the DR1 BAO reconstruction signal as well for the LRG and QSO bins, where we have a power spectrum and bispectrum ShapeFit

measurements, we leave that for future work in order to avoid the complication of determining the exact covariance between BAO and ShapeFit variables [85].

All ShapeFit constraints used in this work include the corresponding systematic error budget.

The data are binned in wavenumber up to a maximum k_{\max} , defined to correspond to mildly non-linear scales, as to retain non-linear information while excluding scales where modelling systematics become significant. We set for our analysis $k_{\max} = 0.15 h \text{ Mpc}^{-1}$ for the power spectrum¹ and $k_{\max} = 0.12 h \text{ Mpc}^{-1}$ for the bispectrum, the latter being the range at which the GEO-FPT model was calibrated [82].

We complement these ShapeFit measurements by adding the reconstructed BAO constraints for the remaining redshift bins, e.g. using the $\alpha_{\text{iso}}(z)$, $\alpha_{\text{AP}}(z)$ measurements and covariances from [23] for the BGS and ELG tracers, and from [24] for the Lyman- α forest.

2.3 Cosmological parameter inference.

The compressed parameters and their covariance, both obtained in [2], are then used to infer cosmological model parameters. The procedure is the following:

1. Given a trial set of cosmological parameters, we compute the predicted ShapeFit parameters ($\alpha_{\text{iso}}(z_{\text{eff}})$, $\alpha_{\text{AP}}(z_{\text{eff}})$, $f(z_{\text{eff}})$, $\sigma_8(z_{\text{eff}})$, $m+n(z_{\text{eff}})$) at each effective redshift, z_{eff} .
2. These predictions are compared to the measured values, and the Gaussian likelihood is computed as

$$\ln \mathcal{L} \propto -\frac{1}{2}(\mathbf{P}_{\text{meas.}} - \mathbf{P}_{\text{th.}})^T \text{Cov}^{-1}(\mathbf{P}_{\text{meas.}} - \mathbf{P}_{\text{th.}}), \quad (2.1)$$

where Cov is the parameter covariance and \mathbf{P} is the vector of parameters, either obtained theoretically or as measured parameters, as in [2].

The steps 1 and 2 are iterated within a Markov Chain Monte-Carlo (MCMC) algorithm², effectively sampling the posterior distribution of cosmological parameters.

In the baseline Λ CDM case, our model parameters are the present matter and baryon physical densities, respectively $\omega_m \equiv \Omega_m h^2$ and $\omega_b \equiv \Omega_b h^2$, the Hubble parameter $h \equiv H_0 \times 10^{-2} [(\text{km/sMpc}^{-1})^{-1}]$, the primordial amplitude of fluctuations, expressed as A_s , and the spectral index n_s . In reporting results we display the matter densities, the Hubble parameter and the amplitude of fluctuations as $\{\Omega_m, \Omega_b, H_0, \ln(A_s \times 10^{10})\}$.

In all cases, the parameters ω_m , h , $\ln(A_s \times 10^{10})$ are sampled with a uniform improper prior. We impose a Gaussian prior of $\omega_b = 0.02218 \pm 0.00055$ following the big bang nucleosynthesis constraints [88]. LSS data is not informative on baryon density and without a ω_b prior either from cosmic microwave background (CMB) or BBN the sound horizon scale remains largely unconstrained.

Additionally, we use a broad Gaussian prior for n_s , equivalent to ten times the Planck 2018 constraints: $n_{s10} = 0.9649 \pm 0.042$. The sum of neutrino masses is fixed to $\sum m_\nu = 0.06 \text{ eV}$ in all cases except in the case where we explore the constraints on the sum of neutrino masses (see Section 3.4). For extended models, we vary the additional relevant parameters:

¹This is a conservative choice, which, however, is not expected to lose significant information. As seen in Fig. 20 of Ref. [3], the recovered constraints are largely insensitive to the choice of k_{\max} within the range from $0.16 - 0.20 h \text{ Mpc}^{-1}$.

²We use the EMCEE [86] algorithm, in four independent runs, and assess convergence with the rank-normalized \hat{R} statistic [87], computed using the ARVIZ package across the four runs. We require $\hat{R} < 1.01$ for all sampled parameters.

e.g., for the (w_0, w_a) model we include those in the parameter vector (with uniform priors); and for free $\sum m_\nu$, we allow it to vary (with a flat prior ≥ 0). All choices of priors are also stated in Table 2.

When combining the DESI clustering measurements with CMB information, we adopt a compressed CMB likelihood defined on the parameter set $\mu_{\text{CMB}} \equiv \{\theta_*, \omega_b, \omega_c\}$, where θ_* is the angular size of the sound horizon at photon decoupling. This likelihood, also used in [89] to extended cosmological scenarios such as $w_0 w_a$ CDM, is modelled as a multivariate Gaussian with mean vector μ_{CMB} and covariance Σ_{CMB} , calibrated from CMB anisotropy measurements following [90]. The mean and covariance take the following values:

$$\mu_{\text{CMB}} \equiv \begin{pmatrix} \theta_* \\ \omega_b \\ \omega_c \end{pmatrix} = \begin{pmatrix} 0.01041 \\ 0.02223 \\ 0.14208 \end{pmatrix}; \quad \Sigma_{\text{CMB}} = 10^{-9} \times \begin{pmatrix} 0.00662 & 0.12440 & -1.19287 \\ 0.12440 & 21.34416 & -94.00083 \\ -1.19287 & -94.00083 & 1488.41710 \end{pmatrix}. \quad (2.2)$$

Model	Parameter	Default	Prior
DESI (Λ CDM)	ω_{cdm}	—	$\mathcal{U}[0.05, 0.2]$
	ω_b	—	$\mathcal{N}[0.02218, 0.00055^2]$
	H_0 [$\text{km s}^{-1} \text{Mpc}^{-1}$]	—	$\mathcal{U}[50, 90]$
	$\ln(10^{10} A_s)$	—	$\mathcal{U}[2, 4]$
	n_s	—	$\mathcal{N}(0.9649, 0.042^2)$
Beyond Λ CDM			
(sound-horizon marginalization)	β	1	$\mathcal{U}[0.5, 2]$
(dynamical DE)	w_0	-1	$\mathcal{U}[-3, 1]$
	w_a	0	$\mathcal{U}[-3, 2]$
(massive ν)	$\sum m_\nu$ [eV]	0.06	$\mathcal{U}[0, 5]$

Table 2. Summary of cosmological parameters considered in this work with their prior ranges. For the scenarios beyond Λ CDM, we also display their default value, which is fixed in the cases where that parameter is not being constrained. For the evolving dark energy equation of state parameters w_0, w_a , the condition $w_0 + w_a < 0$ is imposed, to ensure a period of high-redshift matter domination.

3 Results

3.1 Baseline Λ CDM results

Under the baseline Λ CDM model and for the LRG and QSO samples, the ShapeFit inference from DESI DR1 official measurements [3] yields the orange constraints shown in Figure 1. In that Figure, we also display our results from both the power spectrum-only and the joint power spectrum-bispectrum analysis (respectively in purple and blue) for the same samples, obtained following the methodology described in Section 2. The Planck 2018 Λ CDM central values are reported as the dotted lines, which are within the 1σ region of all posteriors except for H_0 , which is at $\sim 2\sigma$. Interestingly, the addition of the bispectrum shifts the posteriors slightly towards the Planck Λ CDM results (which was also found in an independent analysis of DESI DR1 that also involved the bispectrum, [91]).

The excellent agreement between our power spectrum-only results and the analogous case from the official DESI DR1 results when employing the ShapeFit compression – considering the changes in modelling and pipeline choices – highlights the robustness of these results.

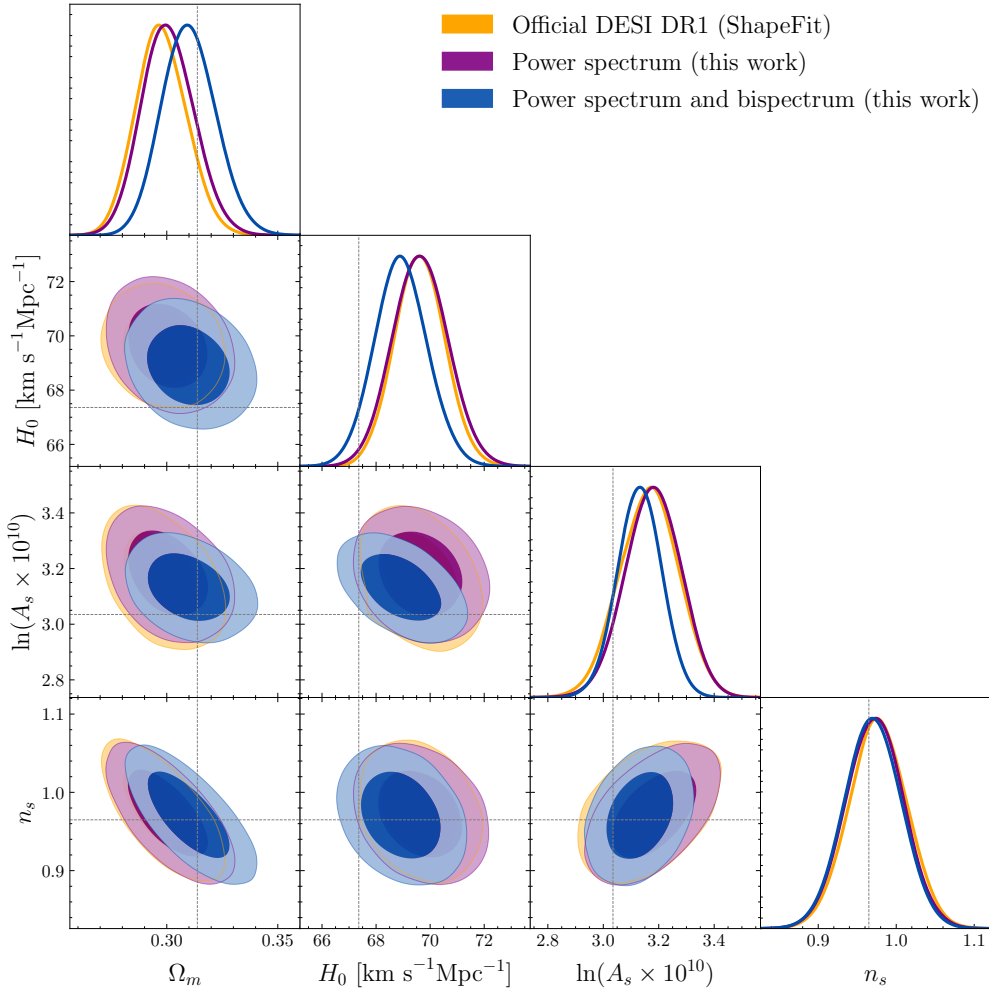


Figure 1. Baseline Λ CDM (68 and 95% confidence levels) joint constraints on the LRG+QSO samples from the DESI DR1 obtained with the ShapeFit compression method, complemented by the BAO postreconstruction data for the BGS, ELGs and Lyman- α tracers. In orange contours, the DESI DR1 official ShapeFit results [3], in purple the results obtained using the methodology of this work (see Section 2) when only using the power spectrum, and in blue when the bispectrum is also added. The horizontal and vertical black dashed lines display the Planck 2018 Λ CDM central values. We note that including the bispectrum leads to constraints on $\ln(A_s \times 10^{10})$ reduced by 20% with respect to the power spectrum-only approach, and that the power spectrum results from this analysis are completely consistent with the ones from the official DESI DR1 analysis.

Adding the bispectrum tightens the constraints for the amplitude of the perturbations parameter $\ln(A_s \times 10^{10})$ by $\sim 20\%$ compared to using the power spectrum alone. In particular,

$$\ln(A_s \times 10^{10}) = \begin{cases} 3.18 \pm 0.10, & \text{for P alone} \\ 3.125 \pm 0.079, & \text{for P+B.} \end{cases} \quad (3.1)$$

The significant reduction in the uncertainty of $\ln(A_s \times 10^{10})$ is achieved through the bispectrum's role in breaking the degeneracy between f and σ_{88} . Similar results were also

found by Ref [91] in an independent analysis of DESI DR1 data when combining the power spectrum bispectrum signals.

The rest of the central values and 68% confident levels are summarized in Table 3.

3.2 Sound-horizon marginalization

A key assumption in standard BAO analyses is that the sound horizon at the drag epoch, r_d , is known from pre-recombination physics (and usually calibrated through ω_b informed by Planck or BBN), and is a derived parameter within the Λ CDM model. Here, we consider the scenario where we drop this assumption, allowing an effective r_d to be a free extra parameter in the fits. Operationally, we follow Ref [92]: in each step of the likelihood exploration we multiply the Λ CDM-inferred r_d parameter by an extra nuisance parameter β . The “new” effective sound horizon scale, $r_d^{\text{eff}} = \beta \times r_d^{\Lambda\text{CDM}}$, is then employed when interpreting the ShapeFit variables such as α_{iso} or σ_{S8} , where we consider a uniform wide prior for β of $\mathcal{U}(0.5, 2)$.

This procedure allows a practical marginalisation over r_d within the ShapeFit formalism, which removes the absolute calibration on the BAO physical scale. Note, however, that the marginalised BAO scale is still exploited in the parameter inference. We still assume that the same effective r_d^{eff} is shared across redshift bins (r_d is z -independent), and that it is an isotropic quantity. This allows us to still employ the BAO scale (with an unknown size) to constrain dimensionless late-time expansion history quantities, such as Ω_m .

In this setup, the cosmological parameters that rely on absolute distance calibrations, such as H_0 , do not depend on the BAO scale anchor, and are “sound-horizon-free”. For the case of a BAO-only analysis, H_0 would remain fully unconstrained. However, there is an additional shape information in the no-wiggle power spectrum, through the transfer-function slope, that provides sensitivity to the equality scale within the ShapeFit framework, the matter-radiation equality scale. This scale arises as a characteristic shape of the matter transfer function in the transition between radiation- and matter-dominated epochs.

Early in the universe’s history, radiation dominance suppressed the growth of matter fluctuations for modes that entered the horizon. Once the universe became matter-dominated, these sub-horizon modes could grow linearly with the scale factor. Because smaller-scale modes entered the horizon earlier (during the radiation era), their growth was delayed relative to larger-scale modes. This results in a transfer function that is nearly flat for large scales ($k < k_{\text{eq}}$) and suppressed for small scales ($k > k_{\text{eq}}$). This transition defines a characteristic scale –the horizon size at matter-radiation equality– which appears as the peak of the linear matter power spectrum at $k_{\text{eq}} \simeq 0.02 h\text{Mpc}^{-1}$.

The exact value of k_{eq} depends on $\Omega_m h^2$ within a late-time Λ CDM model, and it is related to the shape parameter $m + n$, after a prior on n_s and $\Omega_b h^2$ are given. In this case, we keep the same priors as in the standard Λ CDM case displayed in Table 2. Thus, $m + n$ constrains $\Omega_m h^2$ calibrated at the equality scale, and the BAO uncalibrated analysis returns Ω_m , which in combination results in a “sound-horizon-free” determination of H_0 from DESI clustering information alone.

Figure 2 displays the impact of marginalising over the sound horizon scale on the Ω_m – H_0 2D posterior. The blue contours (baseline in this work) assume the standard pre-recombination physics in the sound horizon derivation, $r_d(w_b, w_c, h, \dots)$, while the orange contours (sound-horizon-free) treat the sound horizon scale as a free effective parameter, r_d^{eff} , and marginalise over its value. In the r_d -free case, the contours elongate along the degeneracy $\Omega_m h^2 = \text{constant}$, dominated by the ShapeFit $m + n$ parameter. This degeneracy is only broken when the sound horizon anchor is also used, as in the blue contours. Thus, by

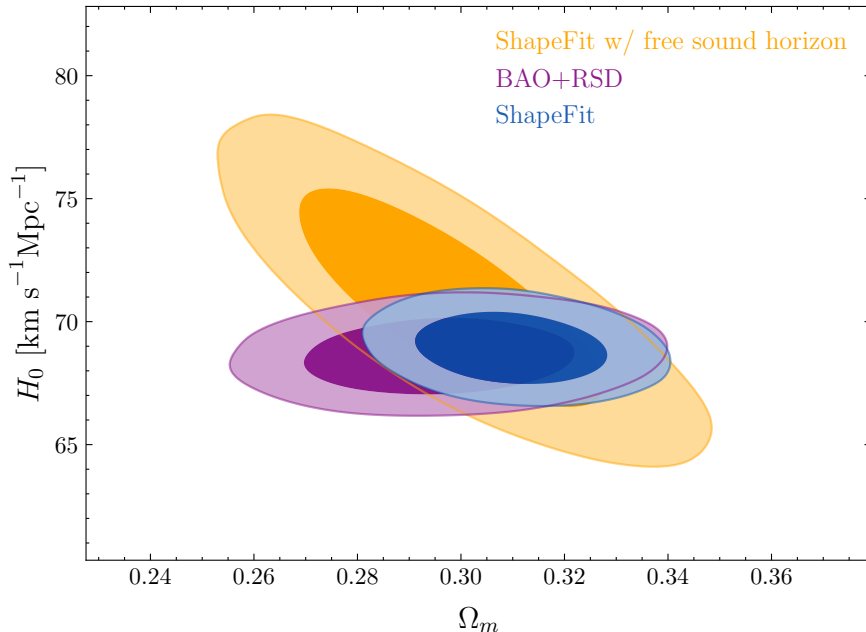


Figure 2. Constraints on Ω_m and H_0 with and without assuming an effective free sound horizon scale parameter r_d^{eff} obtained from the power spectrum and bispectrum ShapeFit results of DESI DR1. The blue contours correspond to the baseline ShapeFit Λ CDM results employing the standard pre-recombination physics $r_d(w_b, w_c, h, \dots)$, which is a derived quantity from the model’s cosmological parameters. The orange contours feature the same analysis settings, except that the sound horizon scale is effectively treated as a free independent parameter and marginalised over, r_d^{eff} . Allowing the horizon scale to freely vary introduces a strong degeneracy between H_0 and Ω_m , which follows $\Omega_m h^2$ degeneracy, and that significantly broadens the H_0 constraints. For completeness, we display in purple contours a similar analysis to the blue contours, but without using the shape parameters $m + n$ (i.e. the so-called standard compression or BAO+RSD).

removing the sound horizon scale anchor, we degrade the precision on the 1-D marginalised H_0 parameter, from $\simeq 1.3\%$ up to $\simeq 5\%$,

$$H_0 [\text{km s}^{-1} \text{Mpc}^{-1}] = \begin{cases} 70.9 \pm 2.9, & \text{sound horizon-free} \\ 68.92 \pm 0.97, & \text{sound horizon-anchored} \end{cases} \quad (3.2)$$

from DESI DR1 clustering alone. The H_0 sound horizon-free result is consistent with both the Planck Λ CDM value and local distance ladder measurements [93, 94]. The sound-horizon free result is also consistent with previous literature on applying this very same methodology to BOSS+eBOSS data [92], as well as with slightly different approaches for sound-horizon-free determinations of H_0 using DESI DR1 data [95, 96].

3.3 Evolving dark energy ($w_0 w_a$)

In this section, we investigate a dynamical dark energy model using the CPL parametrization $w(a) = w_0 + w_a(1 - a)$ [74, 75], with w_0 being the present-day equation-of-state parameter and w_a the parameter describing its evolution with scale factor. This CPL form is a common extension to test whether the data prefer an equation of state different from the cosmological constant value ($w = -1$). Even though it is a phenomenological model, many alternative dark energy scenarios can be expressed in terms of a pair (w_0, w_a) .

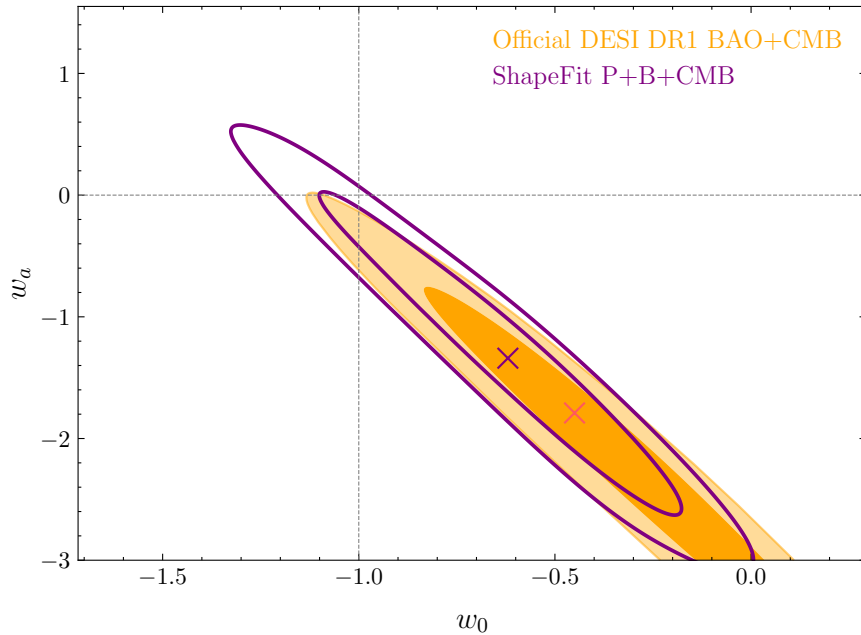


Figure 3. Joint 68 and 95% confidence levels on the dark energy equation-of-state parameters w_0 and w_a from the DESI DR1 power spectrum and bispectrum ShapeFit analysis. The crosses indicate the obtained maximum a posteriori values from the two analyses, and dotted lines indicate the cosmological constant values ($w_0 = -1$, $w_a = 0$). The results are consistent with Λ CDM at the 2σ level, with no significant deviation in either parameter. The slight elongation of the baseline contour reflects the fact that most of the constraining power on the dark energy equation of state comes from the expansion history, which is more tightly constrained by post-reconstruction BAO analyses [7]. The constraints obtained with our methodology (in purple), which use post-reconstruction BAO data for the ELG, BGS and Lyman- α tracers and full-shape information for the LRG and QSO samples, are compared with the official DESI DR1 full post-reconstructed BAO+CMB results from [7].

In this case, we include in our likelihood an additional term relative to the Λ CDM analysis, together with an early-universe prior derived from the Planck CMB likelihood, as described by Eq. 2.2 in Section 2. We allow the parameters w_0 and w_a to vary according to their uniform priors, as shown in Table 2, and obtain the constraints that are shown in Figure 3. We display the 2D posteriors for our full-shape DESI DR1 for $w_0 w_a$ (in purple), compared with the results obtained from the post-reconstruction DESI DR1 BAO analysis [7] (in orange), in both cases for the LRG and QSO bins and with the minimal CMB prior, together with the post-reconstructed BAO data from BGS, ELG and Lyman- α .

We recover the expected degeneracy direction in the $w_0 - w_a$ plane, which arises because the data primarily constrain the effective value of $w(z)$ at the redshift range probed by the observations. As a result, different combinations of w_0 and w_a that yield a similar value of $w(z)$ at that redshift produce nearly identical expansion histories and are therefore degenerate.

The DESI BAO measurements themselves are fully consistent with a cosmological constant Λ ($w_0 = -1$, $w_a = 0$). However, when combined with CMB data they yield a $\sim 3\sigma$ preference away from Λ , a tension that increases if uncalibrated supernovae samples are also added in the data-vector [7]. The Full Shape (ShapeFit) analysis with the inclusion of the bispectrum presented here, constrains the dark energy equation of state to be compatible at 2σ with a cosmological constant Λ : $w_0 = -0.62 \pm 0.29$, $w_a = -1.34 \pm 0.82$, finding no

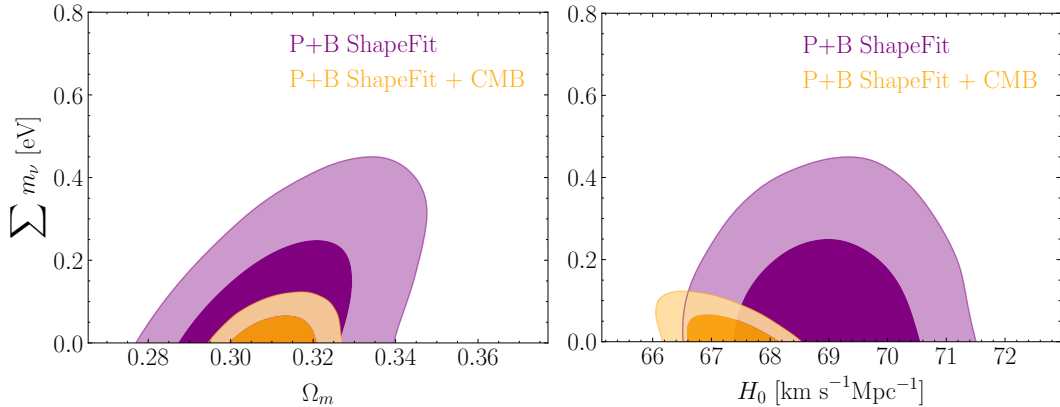


Figure 4. Marginalized posterior for the sum of neutrino masses $\sum m_\nu$ from the DESI DR1 ShapeFit analysis (in purple) together with the constraints of DESI DR1 combined with the compressed Planck likelihood (in orange). This is consistent with previous results, both from the CMB [5] and the DESI collaboration [4, 7], which favour a sum below 100 meV.

significant evidence of dynamical dark energy.

When comparing the recovered errorbars for w_0 and w_a reported in this work with the post-reconstructed BAO+CMB constraints found in [7] (the comparison displayed in Figure 3), we observe both an increase of the errorbars of $\sim 10\%$ with respect to [7], and a shift of $\sim 0.6\sigma$ towards Λ CDM. Both the shift and the elongation of the posteriors of the ShapeFit P+B analysis compared to the BAO ones are in part driven by the effect of reconstruction. The BAO analysis uses reconstruction (which helps tighten the constraints on the expansion history) while the P+B analysis of this work does not use the BAO reconstructed signal for the LRG and QSO samples, as it would require a complete covariance between the ShapeFit and the BAO parameters (see Ref [97] as an example on how to account for such full-covariance).

3.4 Neutrino mass constraints

Massive neutrinos leave an imprint on large-scale structure by suppressing clustering on small scales (which can only be measured in full-shape analyses) and altering the expansion rate (which alters the cosmological distances and therefore has an effect on the BAO). In the baseline analysis, we held the sum of neutrino masses at the value of $\sum m_\nu = 0.06$ eV, and in this Section we allow $\sum m_\nu$ [eV] to vary as a free parameter across the uniform prior $\mathcal{U}[0, 5]$.

Because neutrino mass reduces the amplitude of the power spectrum at small scales (i.e. high k), we expect ShapeFit to be sensitive to it primarily through the shape parameter $m+n$. Still, since the neutrino density was more relevant at early epochs of the expansion history, most of the information on $\sum m_\nu$ is present in pre-recombination probes such as the CMB [7]. We therefore compare the results from DESI DR1 alone with the combination of DESI with the compressed Planck likelihood presented in Section 2.

Figure 4 shows the 2D joint posteriors for $\sum m_\nu$ with the parameters Ω_m and H_0 , respectively. As is common in LSS results, the constraints for $\sum m_\nu$ hit the physical $\sum m_\nu = 0$ prior. We obtain upper limits of respectively,

- $\sum m_\nu < 0.36$ eV (95% DESI DR1),
- $\sum m_\nu < 0.10$ eV (95% DESI DR1+CMB),

which can also be found in Table 3. As expected, DESI DR1 data alone are not sufficiently sensitive to discriminate between neutrino mass hierarchies³. However, when combined with the compressed Planck likelihood, the inverted hierarchy (which requires $\sum m_\nu \gtrsim 0.1$ eV) is disfavoured at approximately the 95% confidence level, whereas the normal hierarchy (with $\sum m_\nu \sim 0.06$ eV) remains consistent with the best-fit results. Our upper bound is comparable to those obtained in previous Planck+LSS analyses, which report limits of order ~ 0.07 eV [4, 7].

4 Discussion

Parameter	Λ CDM	Free r_d	w_0 - w_a (+CMB)	$\sum m_\nu$ (+CMB)
Ω_m	0.310 ± 0.012	0.298 ± 0.020	0.334 ± 0.027	0.3119 ± 0.0064
H_0 [km s ⁻¹ Mpc ⁻¹]	68.92 ± 0.97	70.9 ± 2.9	65.3 ± 2.7	67.13 ± 0.50
$\ln(A_s \times 10^{10})$	3.125 ± 0.079	unconstrained	3.185 ± 0.094	3.207 ± 0.069
w_0	-1^\dagger	-1^\dagger	-0.62 ± 0.29	-1^\dagger
w_a	0^\dagger	0^\dagger	-1.34 ± 0.82	0^\dagger
$\sum m_\nu$ [eV]	0.06^\dagger	0.06^\dagger	0.06^\dagger	< 0.10 (95% CL)

Table 3. Summary of cosmological parameter constraints (maximum a posteriori values and 1σ uncertainties) from DESI DR1 ShapeFit analyses for the joint power spectrum multipoles and bispectrum monopole data-vector, under various scenarios. The columns correspond to: *i*) the baseline Λ CDM model; *ii*) a Λ CDM-like scenario with free sound horizon, r_d ; *iii*) a dynamical dark energy model with free w_0 and w_a ; and *iv*) a model with the total neutrino mass parameter, $\sum m_\nu$, free. In these last two cases, we also add CMB data in the form of the μ_{CMB} data-vector of Equation 2.2, noted as +CMB. The Λ CDM and Free r_d cases use Gaussian priors on ω_b from BBN [88], and in all cases we consider priors for n_s corresponding to 10 times the Planck 2018 constraints [5], as explained in Section 2. For parameters that are not varied in a given scenario, we indicate the fixed value without errorbars with a † symbol (e.g., $w_0 = -1^\dagger$ for baseline Λ CDM). CL stands for confidence levels.

We have presented the cosmological constraints from the DESI DR1 joint power spectrum and bispectrum galaxy clustering data, for both standard Λ CDM and extensions varying the dark energy equation of state and the neutrino mass. We have used the ShapeFit results obtained in [2] from the joint power spectrum and bispectrum data-vector for LRG and QSO tracers, combining them with the reconstructed BAO constraints for BGS and ELG [23], as well as the BAO for the Lyman- α forest from [24]. A summary of results can be found in Table 3, and we highlight the main points in what follows.

For the baseline Λ CDM, we find best-fit parameter values broadly in agreement with both Planck CMB results [5] and the DESI DR1 Full-Shape analysis of the same data [3, 4]: both the matter density Ω_m and amplitude of perturbations $\ln(A_s \times 10^{10})$ are compatible at 1σ with both Planck and DESI DR1 full-shape results. Interestingly, the addition of the bispectrum in the data vector causes the recovered constraints on Ω_m and H_0 to lie closer to Planck than when using only the power spectrum.

The inclusion of the bispectrum in our joint analysis significantly improves the sensitivity to the growth of structure, with errorbars on $\ln(A_s \times 10^{10})$ being reduced by roughly 20%

³We find that when we perform the same analysis without the addition of the bispectrum, $\sum m_\nu < 0.39$ eV (95%), so the inclusion of the bispectrum yields a slight improvement of $\sim 8\%$, when not combining with CMB data.

when the joint data-vector is used. On this parameter alone, adding the bispectrum in the analysis yields equivalent precision improvement as the statistical power gained by using ~ 1.8 times more data.

To further assess the robustness of our H_0 constraints, we also performed an analysis where the sound horizon at the drag epoch, r_d , is treated as a free parameter, following the procedure of [92]. This effectively decouples the low-redshift clustering information from assumptions about early-Universe physics, so marginalizing over r_d allows a more model-independent inference of the Hubble constant. As expected, this leads to a broader posterior, with $H_0 = 71.68 \pm 3.44 \text{ km s}^{-1}\text{Mpc}^{-1}$, compared to $H_0 = 68.92 \pm 0.98 \text{ kms}^{-1}\text{Mpc}^{-1}$ in the baseline ΛCDM case with fixed r_d . The central value shifts upward, while increasing errorbars with respect to [92, 95].

Beyond the baseline model, we explored several extensions (combining with a compressed CMB likelihood), in all cases using the tracer and data-vector choices stated in Section 2, as used also in the ΛCDM case⁴. Allowing the dark energy equation of state parametrized by w_0-w_a , the DESI ShapeFit constraints remain consistent with a cosmological constant. In this parametrization, combining our clustering results with CMB data yields $w_0 \approx -0.6 \pm 0.3$, $w_a \approx -1.3 \pm 0.8$, which is within 2σ of $\Lambda \equiv \{w_0 = -1, w_a = 0\}$. The observed trend –the preference for $w_0 > -1$ and $w_a < 0$, primarily driven by the observed distance measurements in the LRG bins– is similar to that reported in the official DESI BAO and full-shape analyses [4, 7], but is not yet statistically significant in our case.

When allowing the sum of neutrino masses to vary, our ShapeFit analysis (with a compressed *Planck* prior) finds no evidence for a non-zero mass: the posterior is consistent with the minimal mass scenario within normal hierarchy ($\sum m_\nu \approx 0.06 \text{ eV}$). The inverted hierarchy (which requires $\sum m_\nu \gtrsim 0.1 \text{ eV}$) is disfavoured at $\sim 95\%$ confidence by our analysis of DESI DR1 data combined with CMB information. We obtain an upper limit of $\sum m_\nu < 0.1 \text{ eV}$ (95% confidence limits) from ShapeFit, which is slightly weaker than the limit from the DESI full-shape analysis, $\sum m_\nu < 0.071 \text{ eV}$ at 95% confidence limits [4]. The difference can be explained as follows. Firstly, we do not combine full-shape and BAO data in each tracer as we do not dispose of their cross-covariance terms. Neutrino mass weakly affects the expansion history (parametrized by the BAO); additionally, some small-scale clustering information (important for neutrino mass sensitivity) may not be captured by the ShapeFit compression as fully as with the Full Modelling approach.

Overall, across all considered extensions (including time-varying dark energy and massive neutrinos), our analysis shows no strong evidence of new physics beyond ΛCDM , with some results currently being in 2σ tension with Planck.

It is instructive to compare our results with those from the more detailed Full Modelling approaches, specifically with the state-of-the-art DESI Collaboration’s Full Modelling analysis of the same DR1 data [4]. We find agreement between the ΛCDM constraints presented here and the ones presented in [3]. For example, the Full Modelling analysis finds $\{\Omega_m, H_0[\text{kms}^{-1}\text{Mpc}^{-1}], \ln(A_s \times 10^{10})\} = \{0.284 \pm 0.010, 70.0 \pm 1.0, 3.10 \pm 0.10\}$, while we find $\{0.310 \pm 0.012, 68.92 \pm 0.98, 3.125 \pm 0.079\}$.

Our ShapeFit uncertainties (excluding the growth of structure parameter, which is better constrained due to the addition of the bispectrum) are $\sim 10 - 30\%$ larger for parameters such as H_0 , the w_0w_a parametrization or $\sum m_\nu$. These differences in error bars are to be expected:

⁴This yields broader constraints than other results that combine both full-shape and post-reconstruction BAO data for all tracers. In this work, we opt for showing the results without any combination of analyses on any given tracer, and without adding Supernovae data.

in the work presented in this paper, we do not combine the full-shape and the reconstructed BAO information, as done, e.g. in [3]. Such a combination would yield the expansion history and growth of structure to be maximally constrained, but this goes beyond the scope of this paper. Additionally, by construction, ShapeFit compresses the broadband power spectrum information into a few parameters, with a slight loss of information compared to fitting the full shape. This loss is insignificant in the case of Λ CDM, as shown in [3], but can become relevant for extensions of Λ CDM such as the one presented in Section 3.3.

Most importantly, we do not observe any significant bias between Full Modelling analysis on the power spectrum-only data-vector and the Shapefit analysis using both power spectrum and bispectrum: all constraints obtained from ShapeFit are statistically consistent with those from the Full Modelling pipeline, not only for the base Λ CDM parameters but also for the extensions. Both analyses, for instance, report the same qualitative preference for $w_0 > -1$, $w_a < 0$ when DESI is combined with CMB data (Figure 3), and both find neutrino masses to be consistent with the normal hierarchy and constrained to the sub-0.1 eV level.

The ShapeFit methodology has proven to be a powerful yet simple tool for performing cosmological inference in a model-independent way. Its compressed parameter set captures the main cosmological information via the BAO parameters $\alpha_{\text{iso}}, \alpha_{\text{AP}}$, the growth of structure parameters f, σ_{88} , and the shape parameter $m + n$. This comes at the cost of marginally weaker constraints in some beyond- Λ CDM scenarios (due to not directly fitting the full power spectrum), but the simplicity and modularity of ShapeFit have other advantages: one can easily introduce alternate parameters or perform consistency tests (such as freeing the sound-horizon scale r_d to test late-time vs. early-time physics) without re-running a complete model for the power spectra. This is especially useful given that analysing the power spectra or bispectra directly is an increasingly complex task, needing to account for many sources of systematics (see e.g. [2, 3, 76, 98, 99]). Using the ShapeFit compression in a similar way as presented in this paper allows cosmologists, both inside and outside the DESI collaboration, to obtain robust cosmological constraints in a straight-forward way. Moreover, the availability of the intermediate ShapeFit parameters provides a summary of the clustering information that is complementary to Full Modelling approaches, and can help diagnose the origin of possible differences between datasets or between low- and high-redshift probes, particularly in the context of current cosmological tensions (e.g. [6]).

Looking ahead, the DESI survey is expected to increase the survey volume by almost an order of magnitude [100]. The resulting reduction in statistical errors will require refining the methodology to ensure theoretical systematics remain subdominant. Necessary future improvements include modelling the window function for the bispectrum, implementing the θ -cut method for mitigating fibre assignment systematics [99] and updating the strategy to extract the shape parameter m [101].

In conclusion, in this work, we have presented the first joint power spectrum and bispectrum DESI DR1 cosmology results using ShapeFit. While these results do not suggest growing tensions with respect to previous works [4], the constraints are expected to improve significantly as more data are collected. The tools and results shown here can serve as a foundation for those future analyses.

Data Availability

All data from the tables and figures are publicly available in machine-readable format at [10.5281/zenodo.19099550](https://doi.org/10.5281/zenodo.19099550), in compliance with the DESI data management plan.

Acknowledgments

SNM, HGM and LV thank Hernán Noriega, Nicola Deiosso, Uendert Andradea, Benjamin Weaver and Alex Krolewski for the helpful discussion and suggestions. SNM acknowledges funding from the official doctoral programme of the University of Barcelona for the development of a research project under the PREDOCS-UB grant. HGM acknowledges support through the Leonardo programme (LEO23-1-897) of the BBVA foundation and through the programmes Ramón y Cajal (RYC-2021-034104) and Consolidación Investigadora (CNS2023-144605) of the Spanish Ministry of Science and Innovation.

Funding for this work was partially provided by the Spanish MINECO under project PID2022-141125NB-I00 MCIN/AEI, and the ‘Center of Excellence Maria de Maeztu 2020-2023’ award to the ICCUB (CEX2019-000918-M funded by MCIN/AEI/10.13039/501100011033).

This material is based upon work supported by the U.S. Department of Energy (DOE), Office of Science, Office of High-Energy Physics, under Contract No. DE-AC02-05CH11231, and by the National Energy Research Scientific Computing Center, a DOE Office of Science User Facility under the same contract. Additional support for DESI was provided by the U.S. National Science Foundation (NSF), Division of Astronomical Sciences under Contract No. AST-0950945 to the NSF’s National Optical-Infrared Astronomy Research Laboratory; the Science and Technology Facilities Council of the United Kingdom; the Gordon and Betty Moore Foundation; the Heising-Simons Foundation; the French Alternative Energies and Atomic Energy Commission (CEA); the National Council of Humanities, Science and Technology of Mexico (CONAHCYT); the Ministry of Science, Innovation and Universities of Spain (MICIU/AEI/10.13039/501100011033), and by the DESI Member Institutions: <https://www.desi.lbl.gov/collaborating-institutions>. Any opinions, findings, and conclusions or recommendations expressed in this material are those of the author(s) and do not necessarily reflect the views of the U. S. National Science Foundation, the U. S. Department of Energy, or any of the listed funding agencies.

The authors are honored to be permitted to conduct scientific research on I’oligam Du’ag (Kitt Peak), a mountain with particular significance to the Tohono O’odham Nation.

This work has made use of the following publicly available codes: [EMCEE](#) [86], [NUMPY](#) [102], [GETDIST](#) [103], [MATPLOTLIB](#) [104], [ASTROPY](#) [105], [CLASS](#) [106]. We are grateful to the developers who made these codes public.

A The ShapeFit Interpretation Vademecum

In this section, we include a short description on how to interpret the ShapeFit compressed variables in terms of cosmological variables. All this information can be found in existing literature [1, 68, 92], and we refer the reader to those references for further details.

The dilation parameters, $\alpha_{\perp}(z)$ and $\alpha_{\parallel}(z)$ are related to the angular diameter distance, $D_M(z)$, the Hubble distance, $D_H(z)$, respectively, and the sound horizon scale at drag epoch, r_d such that,

$$\alpha_{\parallel}(z) \equiv \frac{D_H(z)/r_d}{[D_H(z)/r_d]_{\text{ref}}}, \quad (\text{A.1})$$

$$\alpha_{\perp}(z) \equiv \frac{D_M(z)/r_d}{[D_M(z)/r_d]_{\text{ref}}}, \quad (\text{A.2})$$

where ref stands for the reference (or fiducial) cosmology at which the redshift-to-distance conversion is performed, and the reference cosmology of the linear power spectrum template. These distances are defined from the Hubble expansion history, $H(z)$, such that,

$$D_H(z) \equiv \frac{c}{H(z)}, \quad (\text{A.3})$$

$$D_M(z) \equiv \frac{c}{H_0 \sqrt{\Omega_k}} \sinh \left[\sqrt{\Omega_k} \int_0^z \frac{dz'}{H(z')/H_0} \right], \quad (\text{A.4})$$

where H_0 is the expansion rate today, $H_0 \equiv H(z=0)$, and Ω_k is the ‘curvature density’ parameter. The sound horizon scale at the drag epoch, r_d depends on pre-recombination parameters, such as the expansion history before recombination, the sound horizon speed in the baryon-photon fluid, and on the redshift of decoupling (or more precisely, the drag epoch, when the baryons stop feeling the presence of the photons). Note how by determining the best-fitting α_{\parallel} and α_{\perp} we can only measure distances in terms of a reference scale: the sound horizon r_d . This is a key point when defining the quantity σ_{ss} below.

The shape parameters m and n parametrize variations of the linear matter template reference such that,

$$P_{\text{lin}}(k) = P_{\text{lin}}^{\text{ref}}(k) \left\{ \frac{m}{a_{\text{SF}}} \tanh \left[a_{\text{SF}} \ln \left(\frac{k}{k_p} \right) \right] + n \ln \left(\frac{k}{k_p} \right) \right\}, \quad (\text{A.5})$$

where the values for a_{SF} and k_p are chosen to be, $a_{\text{SF}} = 0.6$ and $k_p = \pi/r_d^{\text{ref}}$ (although other values could also be chosen). On one hand, the m parameter is the slope at the pivot scale k_p . Within the Λ CDM model, it is related to the $\Omega_m h^2$ parameter, containing information on pre-recombination physics. On the other hand, the n parameter controls the power-law index of the power spectrum at large k values and is related to any effective primordial spectral index, such as the parameter n_s in Λ CDM. In terms of connecting these parameters to the cosmological parameters, we can write the ShapeFit parameter m as [1, 71],

$$m = \frac{d}{d \ln k} \left\{ \ln \left[\frac{P_{\text{lin}, \text{nw}}(k/s)/P_{\mathcal{R}}(k)}{P_{\text{lin}, \text{nw}}^{\text{ref}}(k/s)/P_{\mathcal{R}}^{\text{ref}}(k)} \right] \right\}_{k=k_p}, \quad (\text{A.6})$$

where the subscript ‘nw’ stands for non-wiggle, $P_{\text{lin}, \text{nw}}$ the linear power spectrum with the BAO wiggles filtered out⁵, s is the sound horizon scale in units of its reference value, $s \equiv r_d/r_d^{\text{ref}}$, and $P_{\mathcal{R}}(k)$ is the (power law) primordial power spectrum, $P_{\mathcal{R}}(k) = A_s (k/k_p)^{n_s-1}$, with A_s the primordial amplitude of perturbations and n_s the primordial spectral index. The connection to the second shape parameter, n in this case, is simply,

$$n = n_s - n_s^{\text{ref}}. \quad (\text{A.7})$$

Note that the relation above may differ for cosmologies with non-zero running of the spectral index.

The (logarithmic) growth factor f stands for the logarithmic rate of change of the linear growth parameter $D(a)$ with respect to the logarithm of the scale factor, a ,

$$f(z) \equiv \left. \frac{d \ln D(z')}{d \ln a(z')} \right|_{z'=z}. \quad (\text{A.8})$$

⁵See Appendix B of [68] as well as [101] for a detailed comparison of different smoothing prescriptions.

The amplitude of dark matter fluctuations filtered by an $8 \text{ Mpc} h^{-1}$ scale is usually defined as,

$$\sigma_8^2(z) \equiv \int_0^\infty d^3k P_{\text{lin}}(k, z) W_{\text{TH}}(k \cdot 8 \text{ Mpc} h^{-1}), \quad (\text{A.9})$$

where P_{lin} the linear matter power spectrum, and $W_{\text{TH}}(k \cdot R)$ a top-hat filter with a scale of $R = 8 \text{ Mpc} h^{-1}$ in this case. However, this quantity is not what it is measured by any fixed-template measurement, such as ShapeFit or the traditional compressed method. The traditional compression method (this is the ShapeFit compression where m and n are kept fixed to 0) implicitly assumes an ‘‘early-time rescaling’’, which induces a change in the interpretation of σ_8 via α_{\parallel} and α_{\perp} . Therefore, the actual smoothing scale used to define σ_8 in the equation above is not kept fixed while exploring parameter space during fixed-template fits.

Instead, ShapeFit measures the power spectrum amplitude at a reference scale in units of the sound horizon r_d (recall how the distances D_M and D_H are measured *in terms of* r_d in Eqs A.1-A.2). Additionally, upon changing the shape parameters m and n , the power spectrum amplitude remains fixed only at the pivot scale $k_p = \pi/r_d^{\text{ref}}$; the shape of the power spectrum does change, which in turns affects the σ_8 value. Therefore, in reality, ShapeFit does not constrain σ_8 but effectively constrains the variable $A_{\text{sp}}^{1/2}$, where A_{sp} is the power spectrum amplitude evaluated at k_p/s , which is the quantity that is kept fixed during the parameter exploration,

$$A_{\text{sp}} = \frac{1}{s^3} P_{\text{lin, nw}}(k_p/s). \quad (\text{A.10})$$

Note the overall scaling with $1/s^3$, which appears to describe the volume change when all scales are rescaled by a factor of s (see section 3.1 of [1] for a detailed explanation).

The issue with the definition of σ_8 (i.e., the smoothing scale varying along with other parameters) can easily be accounted for by defining the fluctuation amplitude in such a way that it does not change during the fitting process, i.e., such that it is independent of changes in s , $8 \text{ Mpc} h^{-1} \rightarrow s \cdot 8 \text{ Mpc} h^{-1}$

$$\sigma_{\text{s8}}^2 \equiv \int_0^\infty d^3k P_{\text{lin}}(k, z) W_{\text{TH}}(k \cdot s \cdot 8 \text{ Mpc} h^{-1}). \quad (\text{A.11})$$

Relating A_{sp} to σ_{s8} via $(\sigma_{\text{s8}}/\sigma_{\text{s8}}^{\text{ref}})^2 = A_{\text{sp}}/A_{\text{sp}}^{\text{ref}}$ ignores the changes in the shape of P_{lin} (beyond its overall amplitude) related to the m and n parameters. The exact value of σ_{s8} requires integration over $P_{\text{lin}}(k|m, n)$ at each step of the MCMC sampling of the posterior. A good approximation is given in [92],

$$\left(\frac{\sigma_{\text{s8}}}{\sigma_{\text{s8}}^{\text{ref}}} \right)^2 \simeq \frac{A_{\text{sp}}}{A_{\text{sp}}^{\text{ref}}} \exp \left\{ \frac{m+n}{a_{\text{SF}}} \tanh \left[a_{\text{SF}} \ln \left(\frac{r_d^{\text{ref}} [\text{Mpc} h^{-1}]}{8 \text{ Mpc} h^{-1}} \right) \right] \right\}. \quad (\text{A.12})$$

Note again that ShapeFit can internally work with the parameter A_{sp} (or $f A_{\text{sp}}^{1/2}$) and perform the cosmological interpretation without having to derive σ_{s8} . The only reason to derive σ_{s8} is historical, as to provide a quantity which is similar to the traditional σ_8 parameter, but with a definition that remains consistent and transparent during parameter exploration.

B Sequential ShapeFit compression

We perform the cosmological inference following Section 2 and assuming a Λ CDM model with priors defined in Table 2, using different subsets of the ShapeFit parameters. First, we

analyze the case where only the combined shape parameter $m+n$ is used for the cosmological parameter estimation (shown in yellow in Figure 5). We then derive (Figure 5 in purple) the constraints for its complementary, standard compression, subset consisting of $\alpha_{\text{iso}}, \alpha_{\text{AP}}, f, \sigma_{\text{ss}}$. These results are compared with those obtained using the full ShapeFit framework, which includes both the standard compression parameters and $m+n$ (blue in Figure 5). In all cases, we combine the ShapeFit constraints on the LRG and QSO tracers with the post-reconstructed BAO from BGS, ELG and Lyman- α , as done in all results in the present paper.

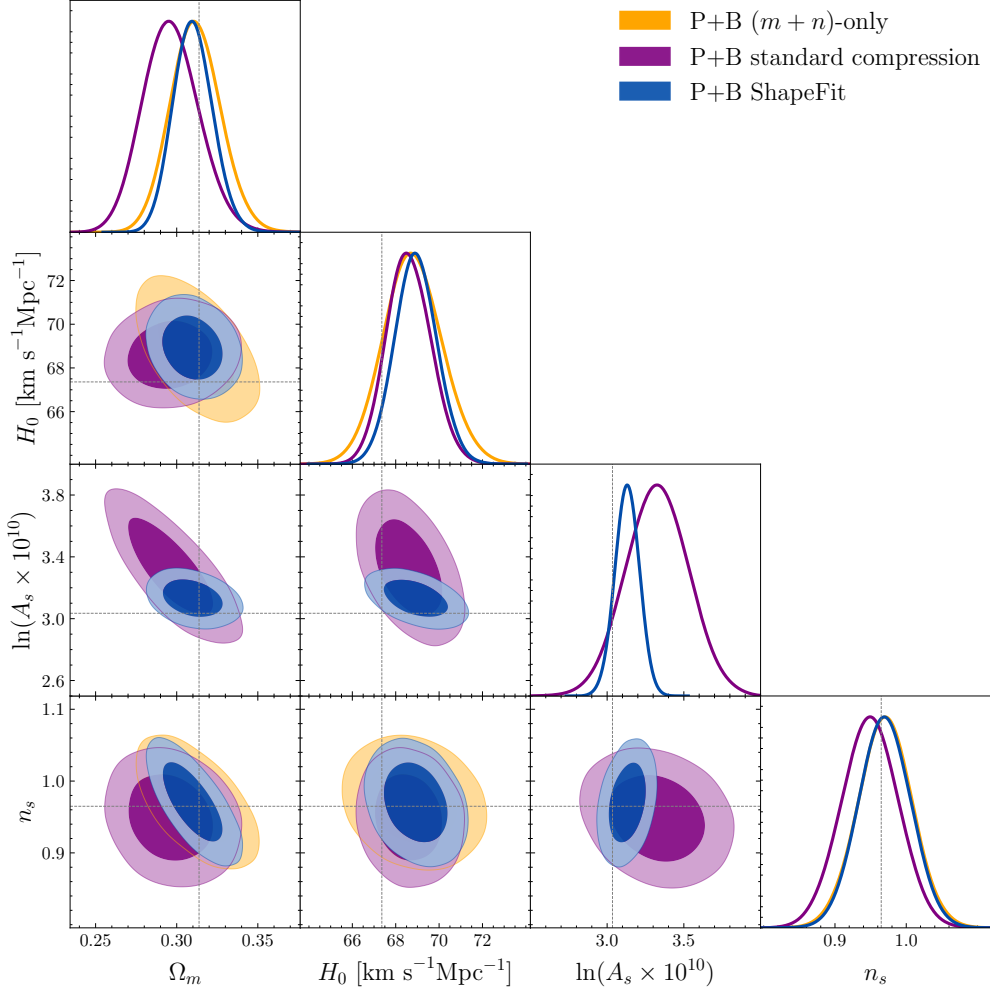


Figure 5. Results for different subsets of the ShapeFit compression. We show marginalized posterior distributions for the Λ CDM parameters Ω_m , H_0 , $\ln(A_s \times 10^{10})$ inferred from the DESI DR1 data using the joint power spectrum-bispectrum analysis. The blue contours correspond to the full ShapeFit analysis (which are therefore identical to the blue constraints in Figure 1). The orange contours use only information from the combined shape parameter $m+n$, while the purple constraints are obtained from the standard compression approach (using the parameters $\alpha_{\parallel}, \alpha_{\perp}, f, \sigma_{\text{ss}}$).

As expected, the full ShapeFit constraints lie approximately at the intersection of the other two cases. Although the shape parameter $m+n$ contains no direct information on the growth of structure, its inclusion significantly reduces the uncertainties in $\ln(A_s \times 10^{10})$ as it breaks the strong degeneracy between Ω_m and $\ln(A_s \times 10^{10})$ present in the standard compression.

C Author Affiliations

- ¹Institut de Ciències del Cosmos (ICCUB), Universitat de Barcelona (UB), c. Martí i Franquès, 1, 08028 Barcelona, Spain.
- ²Institut Químic de Sarrià-Universitat Ramon Llull (IQS-URL), Via Augusta 390, 08017, Barcelona, Spain
- ³Departament de Física Quàntica i Astrofísica, Universitat de Barcelona, Martí i Franquès 1, E08028 Barcelona, Spain
- ⁴Institut d'Estudis Espacials de Catalunya (IEEC), c/ Esteve Terradas 1, Edifici RDIT, Campus PMT-UPC, 08860 Castelldefels, Spain
- ⁵Institució Catalana de Recerca i Estudis Avançats, Passeig de Lluís Companys, 23, 08010 Barcelona, Spain
- ⁶Lawrence Berkeley National Laboratory, 1 Cyclotron Road, Berkeley, CA 94720, USA
- ⁷Department of Physics, Boston University, 590 Commonwealth Avenue, Boston, MA 02215 USA
- ⁸Dipartimento di Fisica “Aldo Pontremoli”, Università degli Studi di Milano, Via Celoria 16, I-20133 Milano, Italy
- ⁹INAF-Osservatorio Astronomico di Brera, Via Brera 28, 20122 Milano, Italy
- ¹⁰Department of Physics & Astronomy, University College London, Gower Street, London, WC1E 6BT, UK
- ¹¹Institute of Space Sciences, ICE-CSIC, Campus UAB, Carrer de Can Magrans s/n, 08913 Bellaterra, Barcelona, Spain
- ¹²Institute for Computational Cosmology, Department of Physics, Durham University, South Road, Durham DH1 3LE, UK
- ¹³Instituto de Física, Universidad Nacional Autónoma de México, Circuito de la Investigación Científica, Ciudad Universitaria, Cd. de México C. P. 04510, México
- ¹⁴NSF NOIRLab, 950 N. Cherry Ave., Tucson, AZ 85719, USA
- ¹⁵University of California, Berkeley, 110 Sproul Hall #5800 Berkeley, CA 94720, USA
- ¹⁶Institut de Física d'Altes Energies (IFAE), The Barcelona Institute of Science and Technology, Edifici Cn, Campus UAB, 08193, Bellaterra (Barcelona), Spain
- ¹⁷Departamento de Física, Universidad de los Andes, Cra. 1 No. 18A-10, Edificio Ip, CP 111711, Bogotá, Colombia
- ¹⁸Observatorio Astronómico, Universidad de los Andes, Cra. 1 No. 18A-10, Edificio H, CP 111711 Bogotá, Colombia
- ¹⁹Institute of Cosmology and Gravitation, University of Portsmouth, Dennis Sciama Building, Portsmouth, PO1 3FX, UK
- ²⁰University of Virginia, Department of Astronomy, Charlottesville, VA 22904, USA
- ²¹Departamento de Física, DCI-Campus León, Universidad de Guanajuato, Loma del Bosque 103, León, Guanajuato C. P. 37150, México
- ²²Fermi National Accelerator Laboratory, PO Box 500, Batavia, IL 60510, USA
- ²³Department of Astronomy, The University of Texas at Austin, 2515 Speedway Boulevard, Austin, TX 78712, USA
- ²⁴Institut d'Astrophysique de Paris. 98 bis boulevard Arago. 75014 Paris, France
- ²⁵IRFU, CEA, Université Paris-Saclay, F-91191 Gif-sur-Yvette, France
- ²⁶Center for Cosmology and AstroParticle Physics, The Ohio State University, 191 West Woodruff Avenue, Columbus, OH 43210, USA

- ²⁷Department of Physics, The Ohio State University, 191 West Woodruff Avenue, Columbus, OH 43210, USA
- ²⁸The Ohio State University, Columbus, 43210 OH, USA
- ²⁹School of Mathematics and Physics, University of Queensland, Brisbane, QLD 4072, Australia
- ³⁰Department of Physics, The University of Texas at Dallas, 800 W. Campbell Rd., Richardson, TX 75080, USA
- ³¹Department of Physics, Southern Methodist University, 3215 Daniel Avenue, Dallas, TX 75275, USA
- ³²Department of Physics and Astronomy, University of California, Irvine, 92697, USA
- ³³Sorbonne Université, CNRS/IN2P3, Laboratoire de Physique Nucléaire et de Hautes Energies (LPNHE), FR-75005 Paris, France
- ³⁴Departament de Física, Serra Húnter, Universitat Autònoma de Barcelona, 08193 Bellaterra (Barcelona), Spain
- ³⁵Instituto Avanzado de Cosmología A. C., San Marcos 11 - Atenas 202. Magdalena Contreras. Ciudad de México C. P. 10720, México
- ³⁶Department of Physics and Astronomy, University of Waterloo, 200 University Ave W, Waterloo, ON N2L 3G1, Canada
- ³⁷Perimeter Institute for Theoretical Physics, 31 Caroline St. North, Waterloo, ON N2L 2Y5, Canada
- ³⁸Waterloo Centre for Astrophysics, University of Waterloo, 200 University Ave W, Waterloo, ON N2L 3G1, Canada
- ³⁹Departament de Física, EEBE, Universitat Politècnica de Catalunya, c/Eduard Maristany 10, 08930 Barcelona, Spain
- ⁴⁰Department of Physics and Astronomy, Sejong University, 209 Neungdong-ro, Gwangjin-gu, Seoul 05006, Republic of Korea
- ⁴¹Abastumani Astrophysical Observatory, Tbilisi, GE-0179, Georgia
- ⁴²Department of Physics, Kansas State University, 116 Cardwell Hall, Manhattan, KS 66506, USA
- ⁴³Faculty of Natural Sciences and Medicine, Iliia State University, 0194 Tbilisi, Georgia
- ⁴⁴CIEMAT, Avenida Complutense 40, E-28040 Madrid, Spain
- ⁴⁵Space Telescope Science Institute, 3700 San Martin Drive, Baltimore, MD 21218, USA
- ⁴⁶Department of Physics, University of Michigan, 450 Church Street, Ann Arbor, MI 48109, USA
- ⁴⁷University of Michigan, 500 S. State Street, Ann Arbor, MI 48109, USA
- ⁴⁸Department of Astronomy, Tsinghua University, 30 Shuangqing Road, Haidian District, Beijing, China, 100190

References

- [1] S. Brieden, H. Gil-Marín and L. Verde, *ShapeFit: extracting the power spectrum shape information in galaxy surveys beyond BAO and RSD*, *J. Cosmology Astropart. Phys.* **2021** (2021) 054 [2106.07641].
- [2] S. Novell-Masot, H. Gil-Marín, L. Verde, J. Aguilar, S. Ahlen, S. Bailey et al., *Full-Shape analysis of the power spectrum and bispectrum of DESI DR1 LRG and QSO samples*, *J. Cosmology Astropart. Phys.* **2025** (2025) 005 [2503.09714].

- [3] A.G. Adame, J. Aguilar, S. Ahlen, S. Alam, D.M. Alexander, M. Alvarez et al., *DESI 2024 V: Full-Shape galaxy clustering from galaxies and quasars*, *J. Cosmology Astropart. Phys.* **2025** (2025) 008 [2411.12021].
- [4] A.G. Adame, J. Aguilar, S. Ahlen, S. Alam, D.M. Alexander, C. Allende Prieto et al., *DESI 2024 VII: cosmological constraints from the full-shape modeling of clustering measurements*, *J. Cosmology Astropart. Phys.* **2025** (2025) 028 [2411.12022].
- [5] Planck Collaboration, N. Aghanim, Y. Akrami, M. Ashdown, J. Aumont, C. Baccigalupi et al., *Planck 2018 results. VI. Cosmological parameters*, *A&A* **641** (2020) A6 [1807.06209].
- [6] L. Verde, T. Treu and A.G. Riess, *Tensions between the early and late Universe*, *Nature Astronomy* **3** (2019) 891 [1907.10625].
- [7] A.G. Adame, J. Aguilar, S. Ahlen, S. Alam, D.M. Alexander, M. Alvarez et al., *DESI 2024 VI: cosmological constraints from the measurements of baryon acoustic oscillations*, *J. Cosmology Astropart. Phys.* **2025** (2025) 021 [2404.03002].
- [8] J.E. Gunn, W.A. Siegmund, E.J. Mannery, R.E. Owen, C.L. Hull, R.F. Leger et al., *The 2.5 m Telescope of the Sloan Digital Sky Survey*, *AJ* **131** (2006) 2332 [astro-ph/0602326].
- [9] W.J. Percival, C.M. Baugh, J. Bland-Hawthorn, T. Bridges, R. Cannon, S. Cole et al., *The 2dF Galaxy Redshift Survey: the power spectrum and the matter content of the Universe*, *MNRAS* **327** (2001) 1297 [astro-ph/0105252].
- [10] K.S. Dawson, D.J. Schlegel, C.P. Ahn, S.F. Anderson, É. Aubourg, S. Bailey et al., *The Baryon Oscillation Spectroscopic Survey of SDSS-III*, *AJ* **145** (2013) 10 [1208.0022].
- [11] K.S. Dawson, J.-P. Kneib, W.J. Percival, S. Alam, F.D. Albareti, S.F. Anderson et al., *The SDSS-IV Extended Baryon Oscillation Spectroscopic Survey: Overview and Early Data*, *AJ* **151** (2016) 44 [1508.04473].
- [12] M. Levi, C. Bebek, T. Beers, R. Blum, R. Cahn, D. Eisenstein et al., *The DESI Experiment, a whitepaper for Snowmass 2013*, *arXiv e-prints* (2013) arXiv:1308.0847 [1308.0847].
- [13] DESI Collaboration, A. Aghamousa, J. Aguilar, S. Ahlen, S. Alam, L.E. Allen et al., *The DESI Experiment Part I: Science, Targeting, and Survey Design*, *arXiv e-prints* (2016) arXiv:1611.00036 [1611.00036].
- [14] DESI Collaboration, A. Aghamousa, J. Aguilar, S. Ahlen, S. Alam, L.E. Allen et al., *The DESI Experiment Part II: Instrument Design*, *arXiv e-prints* (2016) arXiv:1611.00037 [1611.00037].
- [15] DESI Collaboration, B. Abareshi, J. Aguilar, S. Ahlen, S. Alam, D.M. Alexander et al., *Overview of the Instrumentation for the Dark Energy Spectroscopic Instrument*, *AJ* **164** (2022) 207 [2205.10939].
- [16] J.H. Silber, P. Fagrellius, K. Fanning, M. Schubnell, J.N. Aguilar, S. Ahlen et al., *The Robotic Multiobject Focal Plane System of the Dark Energy Spectroscopic Instrument (DESI)*, *AJ* **165** (2023) 9 [2205.09014].
- [17] T.N. Miller, P. Doel, G. Gutierrez, R. Besuner, D. Brooks, G. Gallo et al., *The Optical Corrector for the Dark Energy Spectroscopic Instrument*, *AJ* **168** (2024) 95 [2306.06310].
- [18] J. Guy, S. Bailey, A. Kremin, S. Alam, D.M. Alexander, C. Allende Prieto et al., *The Spectroscopic Data Processing Pipeline for the Dark Energy Spectroscopic Instrument*, *AJ* **165** (2023) 144 [2209.14482].
- [19] E.F. Schlafly, D. Kirkby, D.J. Schlegel, A.D. Myers, A. Raichoor, K. Dawson et al., *Survey Operations for the Dark Energy Spectroscopic Instrument*, *AJ* **166** (2023) 259 [2306.06309].
- [20] R. Zhou, B. Dey, J.A. Newman, D.J. Eisenstein, K. Dawson, S. Bailey et al., *Target Selection and Validation of DESI Luminous Red Galaxies*, *AJ* **165** (2023) 58 [2208.08515].

- [21] DESI Collaboration, A.G. Adame, J. Aguilar, S. Ahlen, S. Alam, G. Aldering et al., *Validation of the Scientific Program for the Dark Energy Spectroscopic Instrument*, *AJ* **167** (2024) 62 [2306.06307].
- [22] DESI Collaboration, A.G. Adame, J. Aguilar, S. Ahlen, S. Alam, G. Aldering et al., *The Early Data Release of the Dark Energy Spectroscopic Instrument*, *AJ* **168** (2024) 58 [2306.06308].
- [23] A.G. Adame, J. Aguilar, S. Ahlen, S. Alam, D.M. Alexander, M. Alvarez et al., *DESI 2024 III: baryon acoustic oscillations from galaxies and quasars*, *J. Cosmology Astropart. Phys.* **2025** (2025) 012 [2404.03000].
- [24] A.G. Adame, J. Aguilar, S. Ahlen, S. Alam, D.M. Alexander, M. Alvarez et al., *DESI 2024 IV: Baryon Acoustic Oscillations from the Lyman alpha forest*, *J. Cosmology Astropart. Phys.* **2025** (2025) 124 [2404.03001].
- [25] A.G. Adame, J. Aguilar, S. Ahlen, S. Alam, D.M. Alexander, M. Alvarez et al., *DESI 2024 II: sample definitions, characteristics, and two-point clustering statistics*, *J. Cosmology Astropart. Phys.* **2025** (2025) 017 [2411.12020].
- [26] C. Poppett, L. Tyas, J. Aguilar, C. Bebek, D. Bramall, T. Claybaugh et al., *Overview of the Fiber System for the Dark Energy Spectroscopic Instrument*, *AJ* **168** (2024) 245.
- [27] M. Abdul-Karim, A. Adame, D. Aguado, J. Aguilar, S. Ahlen, S. Alam et al., *Data release 1 of the dark energy spectroscopic instrument*, *arXiv preprint arXiv:2503.14745* (2025).
- [28] A. Ross, J. Aguilar, S. Ahlen, S. Alam, A. Anand, S. Bailey et al., *The construction of large-scale structure catalogs for the dark energy spectroscopic instrument*, *Journal of Cosmology and Astroparticle Physics* **2025** (2025) 125.
- [29] M. Levi, C. Bebek, T. Beers, R. Blum, R. Cahn, D. Eisenstein et al., *The DESI Experiment, a whitepaper for Snowmass 2013*, *ArXiv e-prints* (2013) [1308.0847].
- [30] A. Raichoor, J. Moustakas, J.A. Newman, T. Karim, S. Ahlen, S. Alam et al., *Target Selection and Validation of DESI Emission Line Galaxies*, *AJ* **165** (2023) 126 [2208.08513].
- [31] E. Chaussidon, C. Yèche, N. Palanque-Delabrouille, D.M. Alexander, J. Yang, S. Ahlen et al., *Target Selection and Validation of DESI Quasars*, *ApJ* **944** (2023) 107 [2208.08511].
- [32] C. Hahn, M.J. Wilson, O. Ruiz-Macias, S. Cole, D.H. Weinberg, J. Moustakas et al., *The DESI Bright Galaxy Survey: Final Target Selection, Design, and Validation*, *AJ* **165** (2023) 253 [2208.08512].
- [33] L. Verde, A.F. Heavens, S. Matarrese and L. Moscardini, *Large-scale bias in the Universe - II. Redshift-space bispectrum*, *Mon. Not. R. Astron. Soc.* **300** (1998) 747 [9806028].
- [34] S. Matarrese, L. Verde and A.F. Heavens, *Large-scale bias in the Universe: bispectrum method*, *MNRAS* **290** (1997) 651 [astro-ph/9706059].
- [35] E. Sefusatti, M. Crocce, S. Pueblas and R. Scoccimarro, *Cosmology and the Bispectrum*, *Phys. Rev. D* **74** (2006) 023522 [astro-ph/0604505].
- [36] J.N. Fry and E. Gaztanaga, *Biasing and Hierarchical Statistics in Large-Scale Structure*, *ApJ* **413** (1993) 447 [astro-ph/9302009].
- [37] C. Hahn, F. Villaescusa-Navarro, E. Castorina and R. Scoccimarro, *Constraining $m\nu$ with the bispectrum. part i. breaking parameter degeneracies*, *Journal of Cosmology and Astroparticle Physics* **2020** (2020) 040.
- [38] A. Oddo, F. Rizzo, E. Sefusatti, C. Porciani and P. Monaco, *Cosmological parameters from the likelihood analysis of the galaxy power spectrum and bispectrum in real space*, *J. Cosmology Astropart. Phys.* **2021** (2021) 038 [2108.03204].
- [39] N. Bartolo, E. Bellini, D. Bertacca and S. Matarrese, *Matter bispectrum in cubic Galileon cosmologies*, *J. Cosmology Astropart. Phys.* **2013** (2013) 034 [1301.4831].

- [40] E. Bellini, R. Jimenez and L. Verde, *Signatures of Horndeski gravity on the dark matter bispectrum*, *J. Cosmology Astropart. Phys.* **2015** (2015) 057 [1504.04341].
- [41] D. Bertacca, A. Raccanelli, N. Bartolo, M. Liguori, S. Matarrese and L. Verde, *Relativistic wide-angle galaxy bispectrum on the light cone*, *Phys. Rev. D* **97** (2018) 023531 [1705.09306].
- [42] H. Gil-Marín, F. Schmidt, W. Hu, R. Jimenez and L. Verde, *The bispectrum of $f(R)$ cosmologies*, *J. Cosmology Astropart. Phys.* **2011** (2011) 019 [1109.2115].
- [43] V. Yankelevich and C. Porciani, *Cosmological information in the redshift-space bispectrum*, *MNRAS* **483** (2019) 2078 [1807.07076].
- [44] W.R. Coulton, J. Liu, M.S. Madhavacheril, V. Böhm and D.N. Spergel, *Constraining neutrino mass with the tomographic weak lensing bispectrum*, *J. Cosmology Astropart. Phys.* **2019** (2019) 043 [1810.02374].
- [45] R. Ruggeri, E. Castorina, C. Carbone and E. Sefusatti, *DEMNUni: massive neutrinos and the bispectrum of large scale structures*, *J. Cosmology Astropart. Phys.* **2018** (2018) 003 [1712.02334].
- [46] P. Gagrani and L. Samushia, *Information Content of the Angular Multipoles of Redshift-Space Galaxy Bispectrum*, *MNRAS* **467** (2017) 928 [1610.03488].
- [47] D. Gualdi and L. Verde, *Galaxy redshift-space bispectrum: the Importance of Being Anisotropic*, *JCAP* **06** (2020) 041 [2003.12075].
- [48] F. Rizzo, C. Moretti, K. Pardede, A. Eggemeier, A. Oddo, E. Sefusatti et al., *The halo bispectrum multipoles in redshift space*, *J. Cosmology Astropart. Phys.* **2023** (2023) 031 [2204.13628].
- [49] M.M. Ivanov, O.H.E. Philcox, G. Cabass, T. Nishimichi, M. Simonović and M. Zaldarriaga, *Cosmology with the galaxy bispectrum multipoles: Optimal estimation and application to BOSS data*, *Phys. Rev. D* **107** (2023) 083515 [2302.04414].
- [50] G. D’Amico, Y. Donath, M. Lewandowski, L. Senatore and P. Zhang, *The one-loop bispectrum of galaxies in redshift space from the Effective Field Theory of Large-Scale Structure*, *J. Cosmology Astropart. Phys.* **2024** (2024) 041 [2211.17130].
- [51] T. Baldauf, U. Seljak and L. Senatore, *Primordial non-Gaussianity in the bispectrum of the halo density field*, *J. Cosmology Astropart. Phys.* **2011** (2011) 006 [1011.1513].
- [52] A. Moradinezhad Dizgah, M. Biagetti, E. Sefusatti, V. Desjacques and J. Noreña, *Primordial non-Gaussianity from biased tracers: likelihood analysis of real-space power spectrum and bispectrum*, *J. Cosmology Astropart. Phys.* **2021** (2021) 015 [2010.14523].
- [53] D. Gualdi, S. Novell, H. Gil-Marín and L. Verde, *Matter trispectrum: theoretical modelling and comparison to N -body simulations*, *J. Cosmology Astropart. Phys.* **2021** (2021) 015 [2009.02290].
- [54] L. Verde and A.F. Heavens, *On the trispectrum as a Gaussian test for cosmology*, *Astrophys. J.* **553** (2001) 14 [astro-ph/0101143].
- [55] R. Scoccimarro, H.A. Feldman, J.N. Fry and J.A. Frieman, *The Bispectrum of IRAS Redshift Catalogs*, *ApJ* **546** (2001) 652 [astro-ph/0004087].
- [56] H. Gil-Marín, J. Noreña, L. Verde, W.J. Percival, C. Wagner, M. Manera et al., *The power spectrum and bispectrum of SDSS DR11 BOSS galaxies - I. Bias and gravity*, *MNRAS* **451** (2015) 539 [1407.5668].
- [57] H. Gil-Marín, L. Verde, J. Noreña, A.J. Cuesta, L. Samushia, W.J. Percival et al., *The power spectrum and bispectrum of SDSS DR11 BOSS galaxies - II. Cosmological interpretation*, *MNRAS* **452** (2015) 1914 [1408.0027].

- [58] H. Gil-Marín, W.J. Percival, L. Verde, J.R. Brownstein, C.-H. Chuang, F.-S. Kitaura et al., *The clustering of galaxies in the SDSS-III Baryon Oscillation Spectroscopic Survey: RSD measurement from the power spectrum and bispectrum of the DR12 BOSS galaxies*, *MNRAS* **465** (2017) 1757 [1606.00439].
- [59] O.H.E. Philcox and M.M. Ivanov, *BOSS DR12 full-shape cosmology: Λ CDM constraints from the large-scale galaxy power spectrum and bispectrum monopole*, *Phys. Rev. D* **105** (2022) 043517 [2112.04515].
- [60] G. D’Amico, Y. Donath, M. Lewandowski, L. Senatore and P. Zhang, *The BOSS bispectrum analysis at one loop from the Effective Field Theory of Large-Scale Structure*, *J. Cosmology Astropart. Phys.* **2024** (2024) 059 [2206.08327].
- [61] G. D’Amico, M. Lewandowski, L. Senatore and P. Zhang, *Limits on primordial non-Gaussianities from BOSS galaxy-clustering data*, *Phys. Rev. D* **111** (2025) 063514 [2201.11518].
- [62] D. Gualdi, H. Gil-Marín, M. Manera, B. Joachimi and O. Lahav, *Geometrical compression: a new method to enhance the BOSS galaxy bispectrum monopole constraints*, *MNRAS* **484** (2019) L29 [1901.00987].
- [63] D. Gualdi, H. Gil-Marín, R.L. Schuhmann, M. Manera, B. Joachimi and O. Lahav, *Enhancing BOSS bispectrum cosmological constraints with maximal compression*, *Mon. Not. Roy. Astron. Soc.* **484** (2019) 3713 [1806.02853].
- [64] G. Cabass, M.M. Ivanov, O.H.E. Philcox, M. Simonović and M. Zaldarriaga, *Constraints on Single-Field Inflation from the BOSS Galaxy Survey*, *Phys. Rev. Lett.* **129** (2022) 021301 [2201.07238].
- [65] G. Cabass, M.M. Ivanov, O.H.E. Philcox, M. Simonović and M. Zaldarriaga, *Constraints on multifield inflation from the BOSS galaxy survey*, *Phys. Rev. D* **106** (2022) 043506 [2204.01781].
- [66] S. Brieden, H. Gil-Marín and L. Verde, *Model-independent versus model-dependent interpretation of the SDSS-III BOSS power spectrum: Bridging the divide*, *Phys. Rev. D* **104** (2021) L121301 [2106.11931].
- [67] S. Brieden, H. Gil-Marín and L. Verde, *PT challenge: validation of ShapeFit on large-volume, high-resolution mocks*, *J. Cosmology Astropart. Phys.* **2022** (2022) 005 [2201.08400].
- [68] S. Brieden, H. Gil-Marín and L. Verde, *Model-agnostic interpretation of 10 billion years of cosmic evolution traced by BOSS and eBOSS data*, *J. Cosmology Astropart. Phys.* **2022** (2022) 024 [2204.11868].
- [69] M. Maus, Y. Lai, H. Noriega, S. Ramirez-Solano, A. Aviles, S. Chen et al., *A comparison of effective field theory models of redshift space galaxy power spectra for DESI 2024 and future surveys*, *J. Cosmology Astropart. Phys.* **2025** (2025) 134 [2404.07272].
- [70] M. Maus, S. Chen, M. White, J. Aguilar, S. Ahlen, A. Aviles et al., *An analysis of parameter compression and Full-Modeling techniques with Velocileptors for DESI 2024 and beyond*, *J. Cosmology Astropart. Phys.* **2025** (2025) 138 [2404.07312].
- [71] H. Noriega, A. Aviles, H. Gil-Marín, S. Ramirez-Solano, S. Fromenteau, M. Vargas-Magaña et al., *Comparing Compressed and Full-Modeling analyses with FOLPS: implications for DESI 2024 and beyond*, *J. Cosmology Astropart. Phys.* **2025** (2025) 136 [2404.07269].
- [72] Y. Lai, C. Howlett, M. Maus, H. Gil-Marín, H.E. Noriega, S. Ramirez-Solano et al., *A comparison between ShapeFit compression and Full-Modelling method with PyBird for DESI 2024 and beyond*, *J. Cosmology Astropart. Phys.* **2025** (2025) 139 [2404.07283].
- [73] S. Ramirez-Solano, M. Icaza-Lizaola, H. Noriega, M. Vargas-Magaña, S. Fromenteau,

- A. Aviles et al., *Full Modeling and parameter compression methods in configuration space for DESI 2024 and beyond*, *J. Cosmology Astropart. Phys.* **2025** (2025) 129 [2404.07268].
- [74] M. Chevallerier and D. Polarski, *Accelerating Universes with Scaling Dark Matter*, *International Journal of Modern Physics D* **10** (2001) 213 [gr-qc/0009008].
- [75] E.V. Linder, *Cosmic growth history and expansion history*, *Phys. Rev. D* **72** (2005) 043529 [astro-ph/0507263].
- [76] R. Gspaner, S. Ramirez-Solano, F. Rodríguez-Martínez, M. Vargas-Magaña, S. Novell-Masot, N. Findlay et al., *Fiducial-Cosmology-dependent systematics for the DESI 2024 Full-Shape Analysis*, *arXiv e-prints* (2025) arXiv:2509.08057 [2509.08057].
- [77] S. Novell-Masot, H. Gil-Marín, L. Verde, J. Aguilar, S. Ahlen, S. Brieden et al., *Catalog-level blinding on the bispectrum for DESI-like galaxy surveys*, *J. Cosmology Astropart. Phys.* **2024** (2024) 089 [2407.12931].
- [78] S. Brieden, H. Gil-Marín, L. Verde and J.L. Bernal, *Blind Observers of the Sky*, *J. Cosmology Astropart. Phys.* **2020** (2020) 052 [2006.10857].
- [79] U. Andrade, J. Mena-Fernández, H. Awan, A. Ross, S. Brieden, J. Pan et al., *Validating the galaxy and quasar catalog-level blinding scheme for the DESI 2024 analysis*, *J. Cosmology Astropart. Phys.* **2025** (2025) 128 [2404.07282].
- [80] H. Gil-Marín, J.E. Bautista, R. Paviot, M. Vargas-Magaña, S. de la Torre, S. Fromenteau et al., *The Completed SDSS-IV extended Baryon Oscillation Spectroscopic Survey: measurement of the BAO and growth rate of structure of the luminous red galaxy sample from the anisotropic power spectrum between redshifts 0.6 and 1.0*, *MNRAS* **498** (2020) 2492 [2007.08994].
- [81] M. Crocce and R. Scoccimarro, *Renormalized cosmological perturbation theory*, *Phys. Rev. D* **73** (2006) 063519 [astro-ph/0509418].
- [82] S. Novell-Masot, D. Gualdi, H. Gil-Marín and L. Verde, *GEO-FPT: a model of the galaxy bispectrum at mildly non-linear scales*, *J. Cosmology Astropart. Phys.* **2023** (2023) 044 [2303.15510].
- [83] N.A. Maksimova, L.H. Garrison, D.J. Eisenstein, B. Hadzhiyska, S. Bose and T.P. Satterthwaite, *ABACUSSUMMIT: a massive set of high-accuracy, high-resolution N-body simulations*, *MNRAS* **508** (2021) 4017 [2110.11398].
- [84] S. Novell-Masot, H. Gil-Marín and L. Verde, *On approximations of the redshift-space bispectrum and power spectrum multipoles covariance matrix*, *J. Cosmology Astropart. Phys.* **2024** (2024) 048 [2306.03137].
- [85] D. Forero-Sanchez, S. Novell-Masot, H. Gil-Marín and L. Verde, *Cosmological constraints from the joint desi dr1 full-shape power spectrum and bispectrum and dr2 bao two-point correlation function, in preparation* .
- [86] D. Foreman-Mackey, D.W. Hogg, D. Lang and J. Goodman, *emcee: The MCMC Hammer*, *PASP* **125** (2013) 306 [1202.3665].
- [87] A. Vehtari, A. Gelman, D. Simpson, B. Carpenter and P.-C. Bürkner, *Rank-normalization, folding, and localization: An improved R-hat for assessing convergence of MCMC (with Discussion)*, *Bayesian Analysis* **16** (2021) 667 [1903.08008].
- [88] N. Schöneberg, *The 2024 BBN baryon abundance update*, *J. Cosmology Astropart. Phys.* **2024** (2024) 006 [2401.15054].
- [89] M. Abdul Karim, J. Aguilar, S. Ahlen, S. Alam, L. Allen, C.A. Prieto et al., *DESI DR2 results. II. Measurements of baryon acoustic oscillations and cosmological constraints*, *Phys. Rev. D* **112** (2025) 083515 [2503.14738].

- [90] P. Lemos and A. Lewis, *CMB constraints on the early Universe independent of late-time cosmology*, *Phys. Rev. D* **107** (2023) 103505 [2302.12911].
- [91] A. Chudaykin, M.M. Ivanov and O.H.E. Philcox, *Reanalyzing DESI DR1: 1. Λ CDM Constraints from the Power Spectrum and Bispectrum*, *arXiv e-prints* (2025) arXiv:2507.13433 [2507.13433].
- [92] S. Brieden, H. Gil-Marín and L. Verde, *A tale of two (or more) h 's*, *J. Cosmology Astropart. Phys.* **2023** (2023) 023 [2212.04522].
- [93] A.G. Riess, W. Yuan, L.M. Macri, D. Scolnic, D. Brout, S. Casertano et al., *A Comprehensive Measurement of the Local Value of the Hubble Constant with 1 km s⁻¹ Mpc⁻¹ Uncertainty from the Hubble Space Telescope and the SH0ES Team*, *ApJ* **934** (2022) L7 [2112.04510].
- [94] H0DN Collaboration, S. Casertano, G. Anand, R.I. Anderson, R. Beaton, A. Bhardwaj et al., *The Local Distance Network: a community consensus report on the measurement of the Hubble constant at 1% precision*, *arXiv e-prints* (2025) arXiv:2510.23823 [2510.23823].
- [95] E.A. Zaborowski, P. Taylor, K. Honscheid, A. Cuceu, A. de Mattia, D. Huterer et al., *A sound horizon-free measurement of H_0 in DESI 2024*, *J. Cosmology Astropart. Phys.* **2025** (2025) 020 [2411.16677].
- [96] E.A. Zaborowski, P. Taylor, K. Honscheid, A. Cuceu, A. de Mattia, A. Krolewski et al., *H_0 Without the Sound Horizon (or Supernovae): A 2% Measurement in DESI DR1*, *arXiv e-prints* (2025) arXiv:2510.19149 [2510.19149].
- [97] D. Forero-Sánchez, H. Gil-Marín, L. Verde, Z. Ding, A.J. Ross, A. Carnero Rosell et al., *Cosmological constraints from a joint DESI DR1 Full-Shape and DR2 BAO*, *arXiv e-prints* (2026) arXiv:2602.18761 [2602.18761].
- [98] N. Findlay, S. Nadathur, W.J. Percival, A. de Mattia, P. Zarrouk, H. Gil-Marín et al., *Exploring HOD-dependent systematics for the DESI 2024 Full-Shape galaxy clustering analysis*, *J. Cosmology Astropart. Phys.* **2025** (2025) 007 [2411.12023].
- [99] M. Pinon, A. de Mattia, P. McDonald, E. Burtin, V. Ruhlmann-Kleider, M. White et al., *Mitigation of DESI fiber assignment incompleteness effect on two-point clustering with small angular scale truncated estimators*, *J. Cosmology Astropart. Phys.* **2025** (2025) 131 [2406.04804].
- [100] R. Besuner, A. Dey, A. Drlica-Wagner, H. Ebina, G. Fernandez Moroni, S. Ferraro et al., *The Spectroscopic Stage-5 Experiment*, *arXiv e-prints* (2025) arXiv:2503.07923 [2503.07923].
- [101] K. Ghaemi, N. Schöneberg and L. Verde, *Smooth sailing or ragged climb? — robustness of power spectrum de-wiggling for ShapeFit parameter compression*, *J. Cosmology Astropart. Phys.* **2025** (2025) 029 [2504.10578].
- [102] C.R. Harris, K.J. Millman, S.J. van der Walt, R. Gommers, P. Virtanen, D. Cournapeau et al., *Array programming with NumPy*, *Nature* **585** (2020) 357 [2006.10256].
- [103] A. Lewis, *GetDist: a Python package for analysing Monte Carlo samples*, *J. Cosmology Astropart. Phys.* **2025** (2025) 025 [1910.13970].
- [104] J.D. Hunter, *Matplotlib: A 2D Graphics Environment*, *Computing in Science and Engineering* **9** (2007) 90.
- [105] Astropy Collaboration, *The Astropy Project: Sustaining and Growing a Community-oriented Open-source Project and the Latest Major Release (v5.0) of the Core Package*, *ApJ* **935** (2022) 167 [2206.14220].
- [106] D. Blas, J. Lesgourgues and T. Tram, *The Cosmic Linear Anisotropy Solving System (CLASS). Part II: Approximation schemes*, *J. Cosmology Astropart. Phys.* **2011** (2011) 034 [1104.2933].